THE JOURNAL OF COMPARATIVE NEUROLOGY 506:161–179 (2008)

Deletion of Voltage-Gated Channel Affects Glomerular Refinement and Odorant Receptor Expression in the Mouse Olfactory System

K.C. BIJU,[1] DAVID RONALD MARKS,[1] THOMAS GERALD MAST,[1] AND DEBRA ANN FADOOL[1,2]*
[1]Department of Biological Science, Program in Neuroscience, Biomedical Research Facility, The Florida State University, Tallahassee, Florida 32306
[2]Department of Biological Science, Programs in Neuroscience and Molecular Biophysics, The Florida State University, Tallahassee, Florida 32306

ABSTRACT

Olfactory sensory neurons (OSNs) expressing a specific odorant receptor (OR) gene send axonal projections to specific glomeruli, creating a stereotypic olfactory sensory map. Odorant receptor sequence, G-protein cAMP signaling, and axon guidance molecules have been shown to direct axons of OSNs toward central targets in the olfactory bulb (OB). Although the OR sequence may act as one determinant, our objective was to elucidate the extent by which voltage-dependent activity of postsynaptic projection neurons in the OB centrally influences peripheral development and target destination of OSNs. We bred OR-tagged transgenic mice to homozygosity with mice that had a gene-targeted deletion of the *Shaker* potassium ion channel (Kv1.3) to elucidate how activity modulates synaptic connections that formulate the sensory map. Here we report that the Kv1.3 ion channel, which is predominantly expressed in mitral cells and whose gene-targeted deletion causes a "super-smeller" phenotype, alters synaptic refinement of axonal projections from OSNs expressing P2, M72, and MOR28 ORs. Absence of Kv1.3 voltage-gated activity caused the formation of small, heterogeneous, and supernumerary glomeruli that failed to undergo neural pruning over development. These changes were accompanied by a significant decrease in the number of P2-, M72-, and MOR28-expressing OSNs, which contained an overexpression of OR protein and G-protein G_{olf} in the cilia of the olfactory epithelium. These findings suggest that voltage-gated activity of projection neurons is essential to refine primary olfactory projections and that it regulates proper expression of the transduction machinery at the periphery. J. Comp. Neurol. 506:161–179, 2008.

Indexing terms: olfactory coding; axon targeting; olfaction; odorant receptor; Kv1.3

The development of precise connectivity and maintenance of an olfactory sensory map is thought to rely upon guidance molecules that are recognized by receptors on olfactory sensory neurons (OSNs) or that are regulated by G-protein-mediated cAMP signals (Bozza et al., 2002; St John et al., 2002; Feinstein et al., 2004; Feinstein and Mombaerts, 2004; Imai et al., 2006; Lattermann et al., 2007; Sweeney et al., 2007). OSNs expressing a given olfactory receptor are primarily randomly dispersed within one of four zones in the main olfactory epithelium (Ressler et al., 1993; Vassar et al., 1993; Mombaerts et al., 1996) but send their axonal projections to spatially conserved glomeruli within the olfactory bulb (Mombaerts, 1996; Wang et al., 1998; Tsuboi et al., 1999). Thus the

Grant sponsor: National Institute of Deafness and Other Communication Disorders, National Institutes of Health; Grant numbers: DC03387 and F31DC008045; Grant sponsor: the Robinson Family & Tallahassee Memorial Hospital; Grant sponsor: Neuroscience Fellowship Award; Grant sponsor: The Florida State University Council on Research and Creativity.

*Correspondence to: Debra Ann Fadool, Ph.D., 214 Biomedical Research Facility, Programs in Neuroscience and Molecular Biophysics, Florida State University, Tallahassee, FL 32306. E-mail: dfadool@bio.fsu.edu

Received 4 June 2007; Revised 15 August 2007; Accepted 11 September 2007

DOI 10.1002/cne.21540

Published online in Wiley InterScience (www.interscience.wiley.com).

olfactory bulb (OB) serves as a two-dimensional map of receptor activation to provide the neural code to discriminate olfactory sensory information (Yu et al., 2004). Odorant quality is thus encoded by a specific combination of activated glomeruli (Mori et al., 1999; Strotmann et al., 2000), and the formation of glomeruli depends on contextual sorting of axons expressing like OR proteins (Belluscio et al., 2002; Feinstein and Mombaerts, 2004; Mombaerts, 2006).

If contextual cues from adjacent homotypic interactions initiate the formation of homogeneous synaptic connections to specific glomeruli, to what degree are these connections fixed under altered electrical activity? Specifically, can altered voltage-dependent activity in central projection neurons perturb the glomerular homogeneity or destabilize the synaptic connections that formulate the sensory map? In the retina, block of voltage-gated sodium channel activity results in pathfinding defects of axonal projections that overshoot their synaptic targets or else acts to retard synaptic strengthening (i.e., Hooks and Chen, 2006). We have examined mice with a gene-targeted deletion of the Kv1.3 ion channel ($Kv1.3^{-/-}$) to understand how voltage-gated activity may influence olfactory coding or organization. In the absence of Kv1.3, mitral cells of the OB have altered action potentials with increased firing frequency, indicating that this channel may regulate the kinetics and timing of neuronal responses to repetitive stimulation (Balu et al., 2004; Fadool et al., 2004). $Kv1.3^{-/-}$ mice also have a heightened sense of smell as defined by behavioral screens for odorant molecular discrimination and odorant threshold detection (Fadool et al., 2004).

We have now generated OR-tagged mice in a Kv1.3-null background by breeding mice with targeted P2- or M72-IRES-tau-lacZ mutations (Mombaerts et al., 1996; Zheng et al., 2000) with mice that have a gene-targeted deletion in the Kv1.3 ion channel. In the absence of Kv1.3 voltage-gated activity, the number of OSNs expressing a particular OR type is drastically reduced, yet the OR patterning in the epithelium does not appear to be altered. In fact, the remaining OSNs appear to have increased transduction machinery at the cilia. In spite of these expression changes, targeting of the OSN axons to the proper region in the bulb is maintained, even though such targeting is through extranumerary connections that are OR-type dependent. In the absence of Kv1.3 voltage-gated activity, axons can coalesce into heterogeneous glomeruli, suggesting that processes that eliminate axons with dissimilar identities are being perturbed and that the refinement of synaptic connections is altered. Thus reported guidance molecules such as semaphorins (Lattermann et al., 2007) play an important instructive role in controlling local axonal convergence into a single glomerulus. However, OR protein expression level and final refinement of synaptic connections (degree of homogeneity of the glomerulus) can be modulated by voltage-gated activity of central projection neurons.

MATERIALS AND METHODS

Solutions and antibodies

Solutions used for protein sample or tissue preparation, namely, nonidet-P40 protease and phosphatase inhibitor (NP40 PPI), homogenization buffer (HB), and phosphate-buffered saline (PBS), were made as described in Tucker and Fadool (2002). The three buffers (A–C) used to visualize β-galactosidase reaction product contained: Buffer A, (0.1 M phosphate buffer, 2 mM $MgCl_2$, 5 mM EGTA; pH 7.4); Buffer B, (0.1 M phosphate buffer, 2 mM $MgCl_2$, 0.01% sodium deoxycholate, and 0.02% Nonidet P40; pH 7.4); Buffer C, (Buffer B with 5 mM potassium ferricyanide, 5 mM potassium ferrocyanide, and 600 μg/ml X-gal). X-gal was purchased from Research Products International (Mt. Prospect, IL). αKv1.3, a rabbit polyclonal antiserum, was generated as a GST-fusion protein with a 53-amino acid peptide (471NSTLSKSMVIEEGGMNHSAFPQTPFKTGNSTATCTTNNNPNDCVNIKKIFTDV523) representing the unique coding region of Kv1.3 on the C-terminus (AB5178, Chemicon, Temecula, CA). The commercial source of αKv1.3 represents an epitope (amino acids 478–523) analogous to that used to generate our αAU13 antiserum, as previously characterized (Tucker and Fadool, 2002). This antiserum was used for both immunocytochemistry (1:500) and Western blot (1:1,000) and did not recognize other *Shaker* family members expressed in the olfactory bulb (Kv1.4, Kv1.5).

Polyclonal antiserum directed against the first putative extracellular loop of mOR256-17 using the peptide sequence LKNLWGPDKTISYGG (Strotmann et al., 2004) was a generous gift from Dr. Heinz Breer (University of Hohenheim, Germany) and was used for Western blot (1:1,000). Specificity controls for α-mOR256-17 included preadsorption with the antigenic peptide and complete overlapping patterns with that generated by in situ hybridization data (Strotmann et al., 2004). Polyclonal antisera effective in detergent-solubilized membrane fractions and histological sections for recognizing mMOR28 (Barnea et al., 2004) were a generous gift from Dr. Richard Axel (Columbia University, New York, NY). α-mMOR28 antisera were generated against two unique epitopes, one in the extracellular domain (residues 167–182) and another in the C-terminal tail domain (residues 302–313). These antisera were previously fully characterized by the Axel laboratory (see online supplemental data in Barnea et al., 2004). Specificity controls for α-mMOR28 included complete overlapping patterns with those generated by β-galactosidase staining using MOR28-IRES-tau-LacZ mice. Lack of antibody staining was also confirmed in isolated membrane fractions of adult main olfactory epithelium (MOE) in mice with a gene-targeted deletion of MOR28. Immunoprecipitated MOR28 from wild-type mice also demonstrated a predicted band shift following expected glycoprotein enzymatic cleavage. Further analysis was completed by using myelin basic protein (MBP)-based MOR28 fusion proteins to demonstrate both expected size/mobility and band specificity (Barnea et al., 2004).

Olfactory marker protein (OMP) antiserum was purchased from Wako (Richmond, VA, cat. #544-10001), and β-galactosidase antiserum was purchased from Rockland Immunochemicals (Gilbertsville, PA, cat. #200-4136). Goat anti-OMP (α-OMP) was generated as originally described by Keller and Margolis (1975) by using homogeneous full-length OMP isolated from rat olfactory tissue; its specificity has been widely tested across many animal phyla by using extensive controls such as radioimmunoassay (RIA), preadsorption with antigenic peptide, and labeling comparison with genetically-modified mice linked with reporters such as LacZ, GFP, or EGFP-AdV (i.e., Walters et al., 1996; Ivic et al., 2000). Although it is highly

specific for mature olfactory neurons and their axons, it also demonstrates labeling of a few select central neurons throughout the brain (Baker et al., 1989). The immunogen for α-β-galactosidase was the enzyme derived from *E. coli*, which was purified by a multistep process including ion exchange chromatography and extensive dialysis to create a suitable product for a broad range of immunodetection procedures (ELISA, Western blot, immunocytochemistry, immunoprecipitation). Both of these antisera were used at 1:1,000 for confocal imaging experiments.

Finally, anti-$G_{\alpha olf}$ (1:1,000) was a generous gift from Dr. Albert Farbman (Northwestern University, Evanston, IL), who generated the antiserum by using the same antigen as Reed's antiserum (CY coupled to KTAEDQGVDEKERREA, near the amino terminus of rat G_{olf}; Jones and Reed, 1989). The specificity of anti-$G_{\alpha olf}$ has been previously confirmed at both the light microscope and ultrastructural level by using preadsorption and omission of primary antiserum; it was found to label predominantly olfactory cilia of mature OSNs (Mania-Farnell and Farbman, 1990; Menco et al., 1994).

Generation of mice carrying targeted mutations

Kv1.3-null ($^{-/-}$) mice were generated previously by deleting a large promoter region and the N-terminal third of the Kv1.3 coding sequence (Koni et al., 2003; Xu et al., 2003). These mice were generously provided by Drs. Leonard Kaczmarek and Richard Flavell (Yale University, New Haven, CT). P2-IRES-tau-LacZ and M72-IRES-tau-LacZ mice were generated previously via placement of an internal ribosome entry site (IRES) directing the translation of tau:lacZ fusion protein immediately downstream of the P2 or M72 odorant receptor stop codon (Mombaerts et al., 1996; Zheng et al., 2000). These mice were a generous gift from Dr. Peter Mombaerts (Rockefeller University, New York, NY). OSNs of these mice that express the modified P2 or M72 receptors can be visualized by histological staining for β-galactosidase activity along with the odorant receptor (Mombaerts et al., 1996; Zheng et al., 2000). We generated odorant receptor-tagged mice in a Kv1.3-null background by breeding homozygous P2- or M72-IRES-tau-LacZ mice with homozygous Kv1.3$^{-/-}$ mice. The resultant double heterozygous animals in the F1 generation were interbred to establish the double mutation (P2Kv1.3$^{-/-}$ or M72Kv1.3$^{-/-}$) at expected Mendelian inheritance probabilities. All F2 double-mutant mice were outcrossed with wild-type mice to confirm homozygosity of both mutant alleles and thus ensure accuracy of polymerase chain reaction (PCR)-based genotyping.

All mice were housed at the Florida State University vivarium with a 12/12-hour light/dark cycle and in accordance with institutional requirements for animal care. Cage design has been reported to affect bulbar development and topography as well as animal behavior, such as aggression (Restrepo, unpublished data). All mice in our study were individually housed in conventional-style rodent cages containing separate water and food that could be obtained ad libitum. Cage tops were not outfitted with HEPA filtration or individual ventilation (IVC), but room air circulation was standardized at 19 changes/hour, and soiled litter was replaced once or twice weekly.

For simplicity, the following nomenclature will be used throughout the manuscript: P2-IRES-tau-LacZ (WTP2), M72-IRES-tau-LacZ (WTM72), Kv1.3-null P2-IRES-tau-LacZ double-homozygous mutant mice (KvP2), and Kv1.3-null M72-IRES-tau-LacZ double-homozygous mutant mice (KvM72). All genetically-modified mice were established by using a B6C57 genetic background. The number of generations since the founder was as follows: sixth through ninth (KvP2) and fifth through eighth (KvM72). Some transgenic lines were gifts to the investigators (sources as previously noted) and founder generation is not known, but the lines have been maintained in our colony and were used experimentally over the following generations: 6th–8th (WTP2), 4th–6th (WTM72), and 11th–13th (Kv1.3$^{-/-}$). The number of backcrosses to each inbred strain ranged from two to four. The age and number of animals used for each experimental group are given in the Results. Experiments contained animals of both sexes.

X-Gal staining

Mice were sacrificed with an overdose of sodium pentobarbital and perfused with 4% paraformaldehyde as per Florida State University Laboratory Animal Resources and AVMA-approved methods. Heads were decalcified in 0.3 M EDTA for 48 hours at 4°C. Both the nasal epithelium and olfactory bulbs were exposed and rinsed in PBS. A total of 151 animals across the four genotypes (WTP2, WTM72, KvP2, KvM72) and ranging from postnatal day 10 (P10) to 2 years of age were processed for either whole-mount staining or for cyrosectioning as previously described (Mombaerts et al., 1996). Briefly, both tissue preparations were washed with Buffer A for 5 minutes and then again for 25 minutes at room temperature (RT). Tissues were then incubated twice with Buffer B for 5 minutes each, followed by a 6-hour incubation in Buffer C at RT. Whole mounts were examined with a Leica MZ FLIII stereomicroscope (Wetzlay, Germany) and images were acquired with an Olympus DP10 digital camera (Tokyo, Japan). Cryosections were counterstained with neutral red following the X-gal processing described above to visualize targets of projections and number and distribution of P2- or M72-expressing OSNs by light photomicroscopy (Zeiss, Oberkochen, Germany, Axiovert S 100). Digital images were captured by using a Zeiss Axiocam digital camera and AxioVision software and then processed with Adobe Photoshop CS (San Jose, CA). At least five sets of coronal serial, MOE sections (16-μm thickness) were used to quantify P2- and M72-expressing OSNs from postnatal day 20 OR-tagged mice of wild-type (Kv1.3$^{+/+}$) or channel-deficient (Kv1.3$^{-/-}$) genotype. Manual counts of positively identified OR-expressing OSNs were statistically compared (plus or minus channel) by using a Student's *t*-test at the 95% confidence level ($p \leq 0.05$). Unless otherwise stated, all data are reported as the mean ± standard error of the mean (SEM).

Double-color immunofluorescence

Olfactory bulbs were fixed in 4% paraformaldehyde, cryoprotected in 30% sucrose, and coronally sectioned at 60-μm thickness (Leica CM1850). Sections were prepared for sequential double-labeling by using non-crossreacting, host-specific polyclonal antisera. In brief, sections were rinsed in PBS and incubated overnight in the first primary antibody (anti-β-galactosidase or anti-MOR28; see Solutions and antibodies) followed by a 2-hour incubation in fluorescein isothiocyanate (FITC)-conjugated anti-rabbit IgG (1:100). Unbound antibody was rinsed in PBS for 30

minutes and sections were incubated overnight in the second primary antibody (anti-OMP) followed by a 2-hour incubation in Texas Red-conjugated anti-goat IgG (1:100). This was followed by a wash in PBS and a 5-minute incubation with the nuclear stain 4,6-diamidino-2-phenylindole (DAPI; 1:5,000). Sections were rinsed, coverslipped in Vectashield (Vector, Burlingame, CA), and imaged by using a Zeiss (Thornwood, NY) LSM510 two-photon confocal system. Serial optical sections were captured at 1-μm intervals and were saved as three-dimensional stacks. The images were then imported into Adobe Photoshop CS, where image brightness and contrast were adjusted for maximal clarity.

Similar immunofluorescence procedures were performed for the olfactory epithelium with slight modifications to visualize just a single epitope (by using polyclonal antisera to MOR28 or G_{olf} G-protein) on sections cut to 16-μm thickness.

Scanning electron microscopy

Receptor untagged wild-type and Kv1.3$^{-/-}$ mice (P20) were perfused transcardially with chilled PBS followed by 2.5% glutaraldehyde containing 2% paraformaldehyde in 0.1 M phosphate buffer (pH 7.4). The olfactory turbinates were dissected out and retained in the same fixative overnight at 4°C. After rinsing in phosphate buffer, specimens were dehydrated in a graded series of acetone, critical-point-dried from CO_2, and then sputtered with gold-palladium (Au-Pd alloy; Dawes, 1984). The samples were examined with an FEI Nova NanoSEM 400 (Hillsboro, OR). Secondary electron images were obtained at 10-kV accelerating voltage by using a horizontal field width (HFW) between 13.6 and 15.7 μm and at magnifications ranging from 10,000 to 15,000×.

Biochemistry

Postnatal day (P) 20 mice were euthanized by CO_2 inhalation as per Florida State University Laboratory Animal Resources and AVMA-approved methods, and the MOE was quickly harvested after decapitation. The MOE was immediately homogenized in HB for 50 strokes with a Kontes (Kimble Chase, Vineland, NJ) tissue grinder (size 20) on ice. HB-processed epithelia were used to isolate membrane proteins as previously described (Tucker and Fadool, 2002). Protein concentrations were determined by a Bradford assay (Bio-Rad, Hercules, CA), and samples were stored at −80°C until subsequent use.

Membrane proteins (20–30 μg/lane) were separated on 8–10% acrylamide gels by sodium dodecyl sulfate-polyacrylamide gel electrophoresis (SDS-PAGE) and electrotransferred to nitrocellulose blots as previously described (Cook and Fadool, 2002; Tucker and Fadool, 2002; Fadool et al., 2004). Enhanced chemiluminescence (ECL; Amersham Biosciences, Buckinghamshire, UK) exposure on Fugi Rx film (Fisher Scientific, Suwannee, GA) was used to visualize labeled proteins. The film autoradiographs were analyzed by quantitative densitometry by using a Hewlett-Packard PhotoSmart Scanner (model 106-816, Hewlett Packard, San Diego, CA) in conjunction with Quantiscan software (Biosoft, Cambridge, UK). Immunodensity ratios (Kv1.3$^{-/-}$ over wild type) were calculated for proteins from SDS gels electrophoresed together, electro-transferred to the same piece of nitrocellulose, and exposed to the same piece of X-ray film to standardize any variance in transfer or ECL exposure. Normalized immunodensity values for a given visualized protein were compared across genotype by using an Arc-Sin transformation for percentage data with a Student's *t*-test at the 95% confidence level.

RESULTS

Lack of expression of Kv1.3 channel protein in the MOE

To test whether Kv1.3 was expressed by OSNs, we applied both immunocytochemical and biochemical approaches to demonstrate control levels of expression of the channel in the olfactory system of wild-type animals. mRNA encoding Kv1.3 has not been detected by in situ hybridization approaches applied to the MOE but has been found to be strongly expressed in both the OB and piriform cortex (Kues and Wunder, 1992). To rule out either transient or developmental expression of the channel protein in the MOE, we surveyed MOE cryosections and purified membrane preparations from early postnatal stages through adult (P1–P41). As shown in Figure 1A–NN, we were not able to detect Kv1.3 in the sensory epithelium at high magnification nor did the antiserum label an appropriate size molecular weight protein (55–66 kDa depending on phosphorylation state) under denatured conditions (Fig. 1TT). At lower magnification we were also not able to visualize αKv1.3 labeling across any cell types of the MOE including the lamina propria and the axon cell bundles in any developmental age, as shown in the representative sections acquired at P41 (Fig. 1OO–QQ). We utilized detection of another membrane-bound protein, known to be enriched in the MOE (G_{olf}) and the detection of the channel in the OB, as positive controls for immunolocalization in our prepared sections and membranes, respectively (Fig. 1A–NN, first column; Fig. 1RR–SS). We additionally used cloned Kv1.3 heterologously expressed in HEK 293 cells as a migration standard to demonstrate specificity of the αKv1.3 antibody, which was previously well characterized in native OB by immunocytochemistry and Western analysis (Fadool et al., 2000; Tucker and Fadool, 2002; Fadool et al., 2004; Marks and Fadool, 2007).

Specificity of axonal projections in Kv1.3-null mice

Kv1.3-null P2-IRES-tau-LacZ double-homozygous mutant mice (KvP2) and Kv1.3-null M72-IRES-tau-LacZ double-homozygous mutant mice (KvM72) were generated as described (see Materials and Methods). Patterns of projections from P2- and M72-expressing OSNs were analyzed in whole-mount preparations of postnatal day 20 animals (P20). Due to differences in brain size (brain/body weight ratio: wild type 0.06 ± 0.01 vs. Kv1.3$^{-/-}$ 0.04 ± 0.01, significantly different by Student's *t*-test, $n = 8$, $p \leq 0.05$), olfactory bulb size, and size and number of glomeruli between wild-type and Kv1.3$^{-/-}$ mice (Fadool et al., 2004; Biju et al., 2006) it was not possible to determine precisely whether specific P2- or M72-expressing neurons of Kv1.3$^{-/-}$ mice converged to the exact glomerulus as that reported for wild-type animals (referred to as WTP2 and WTM72, respectively). The approximate location of the axonal projections, however, was not markedly different between WTP2 vs. KvP2 or between WTM72 vs. KvM72 (Fig. 2). Albeit at the expected location, axons of

the M72 neurons in the KvM72 mice did not converge as a tight glomerular organization but rather projected as multiple extraglomerular positions (Fig. 2D).

In contrast, it appeared that the P2 neurons converged on a single glomerulus on both the medial and lateral aspect of the OB. Although this was examined for 15 WTP2 (Fig. 2A) vs. that for 15 KvP2 animals (Fig. 2B), we could not be certain of the exact organization of this projection due to the deep position of the P2 glomerulus. Rather than rely solely on examination of the whole-mount orientation, we histologically labeled for β-galactosidase in serial coronal sections of the OB. Our detailed serial section analysis in WTP2 mice revealed that axons typically terminated in one to three glomeruli per OB (Fig. 3A). Three of ten WTP2 mice examined had four glomeruli in either the right or left OB. In KvP2, however, each OB had four to six glomeruli (Fig. 3B). The extra P2 glomeruli in the KvP2 mice showed no consistency in location, many were smaller, and most only partially innervated the targeted glomerulus.

Due to the generous availability of an antiserum to the MOR28 OR, we were able to compare the organization of the P2 and M72 glomeruli with that of the MOR28 glomerulus. Serial coronal sections of OB from receptor untagged wild-type and Kv1.3$^{-/-}$ animals were immunostained with an antibody directed against an extracellular epitope of the mouse odorant receptor MOR28. In both wild-type and Kv1.3$^{-/-}$ animals, the antibody labeled only two glomeruli, one medial and one lateral, in the ventral aspect of the OB (Fig. 3C,D). Thus, across the three types of glomeruli examined, the number of axonal projections in the Kv1.3$^{-/-}$ background appeared to be OR-type dependent.

Because the relative positions of glomeruli are thought to remain fixed throughout the life of an organism (Mombaerts, 1996; Wang et al., 1998; Tsuboi et al., 1999; St. John et al., 2002), yet can undergo synaptic pruning over the course of development (Royal and Key, 1999), we questioned whether the M72 and P2 glomerular organizations were simply delayed in the Kv1.3-null mice or whether the extraglomerular connections were relatively fixed for these OR-specific projections. Eighty-three mice were examined as distributed across all genotypes (WTM72, KvM72, WTP2, KvP2) and four postnatal ages (P8–P14, P20, P30, and greater than 1 year) for M72 or two postnatal ages (P20 and 2 years) for P2. As shown in representative photomicrographs of whole-mount β-galactosidase staining for the M72 glomerulus in Figure 4A–J, the extraglomerular connections were observed independent of age of development, suggesting that altered voltage-gated activity in mitral cells altered fine refinement of the connection rather than delayed the time until synaptic convergence to a single locus. The minimum and maximal number of M72 and P2 glomeruli per OB are reported in Figure 4K and L, respectively. Although all KvM72 and KvP2 mice had a greater number of glomeruli than that of their wild-type counterparts, the number of M72 or P2 glomeruli at postnatal day 20 was subject to statistical comparison due to population size (availability of transgenics) and was found to be significantly greater by Student's *t*-test: M72 = 4.17 ± 0.19 glomeruli/bulb for KvM72 (n = 28) vs. 2.4 ± 0.16 glomeruli/bulb for WTM72 (n = 10); $p \leq 0.05$; P2 = 5.0 ± 0.23 glomeruli/bulb for KvP2 (n = 5) vs. 3.1 ± 0.21 glomeruli/bulb for WTP2 (n = 5); $p \leq 0.05$.

Heterogeneous glomeruli in Kv1.3-null mice

During neuronal development, it is believed that olfactory axons sort themselves by heterophilic (repulsive) interactions. There is also evidence which demonstrates that OR amino acid sequence gives the OSN axons the ability to coalesce into glomeruli by homophilic interactions (Feinstein and Mombaerts, 2004). OSN axons are found to be highly precise in targeting glomeruli, and glomeruli are highly homogeneous with regard to the OR expressed by the innervating OSNs (Treloar et al., 2002). We used a strategy of double-color immunofluorescence to investigate the role of voltage-gated activity in the development of glomeruli innervated by axons from OSNs expressing a single type of OR (homogeneous glomeruli). Sixty-micron-thick cryosections of the OB were prepared from WTP2, KvP2, WTM72, KvM72, and receptor untagged wild-type and Kv1.3$^{-/-}$ mice. Sections were sequentially labeled with a host-specific antiserum for olfactory marker protein (OMP), to label all mature olfactory sensory neurons and their axonal projections to the olfactory bulb, and for β-galactosidase (to identify the M72 or P2 glomerulus) or MOR28 (to identify the MOR28 glomerulus). In homogeneous M72, P2, and MOR28 glomeruli, immunoreactivity for OMP should largely overlap with either β-galactosidase or MOR28 immunoreactivity, respectively.

As expected and shown for two representative WTM72 mice in Figure 5 (A–C, D–F), the merged two-photon, confocal image indicates that the innervation of the M72 glomerulus contains projections that appear to be solely derived from axons of M72-expressing OSNs (statistically compared in Fig. 5Y). By comparison, however, and shown for two representative KvM72 mice in Figure 5 (G–I, J–L), the merged confocal image indicates that the M72 glomerulus is only partially innervated by axons of M72-expressing OSNs (green channel) and that a proportion of the glomerulus is labeled with axons that are OMP positive, β-galactosidase negative (red channel; see also Fig. 5Y). These data suggest that lack of voltage-gated activity disrupts the homophilic interactions among OSN axons of like OR identity and that the result is formation of a heterogeneous glomerulus, innervated by at least two different OSN types or at least another OSN not expressing M72 OR. In WTP2 mice, at P20, the majority of axons in the P2 glomerulus exhibited colocalization of OMP and β-galactosidase immunoreactivity (Fig. 5M–O). At this age, a few axons targeting the P2 glomerulus exhibited OMP-positive, β-galactosidase-negative immunoreactivity (Fig. 5T). In KvP2, however, the proportion of OMP-positive, β-galactosidase-negative axons was significantly greater than that which showed colocalization of both OMP and β-galactosidase (Fig. 5P–R,Z). Persistence of a few OMP-positive, β-galactosidase-negative fibers in WTP2 mice at P20 may indicate that P2 glomeruli may require more than 20 days to mature. Glomerular maturation has been shown to be OR-type dependent (Zou et al., 2004); M71 glomeruli, for example, do not reach synaptic maturity until P60. In contrast, M72 glomeruli mature as early as P20 (Zou et al., 2004). Finally, in receptor untagged wild-type mice, two-color immunofluorescence using αOMP and αMOR28 revealed completely overlapping axons in MOR28 glomeruli. In contrast, MOR28 glomeruli in a Kv1.3$^{-/-}$ background, as with P2 and M72, exhibited heterogeneity, with an equivalent, increased

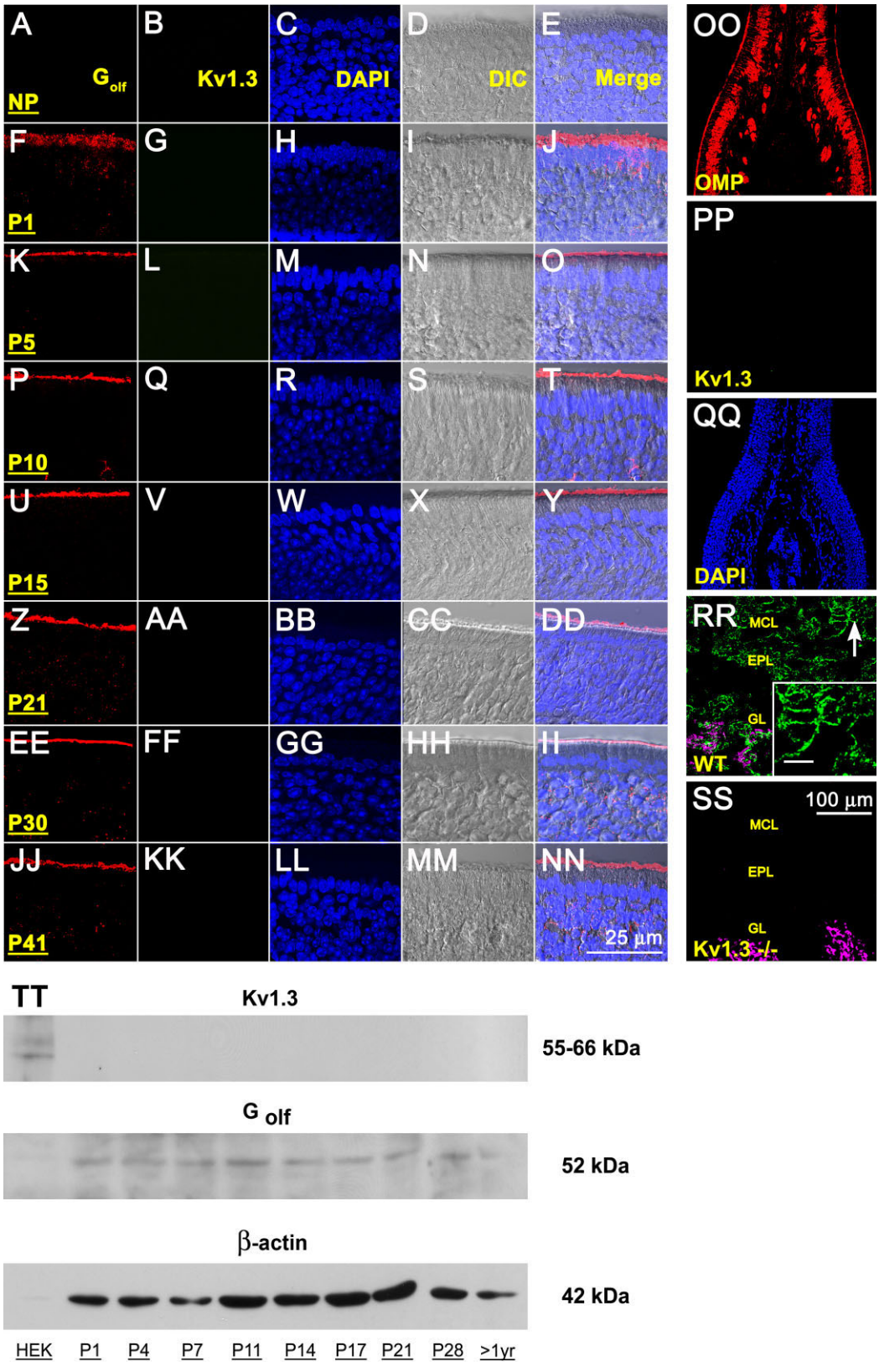
A
G olf
NP
B
Kv1.3
C
DAPI
D
DIC
E
Merge
F
P1
G
H
I
J
K
P5
L
M
N
O
P
P10
Q
R
S
T
U
P15
V
W
X
Y
Z
P21
AA
BB
CC
DD
EE
P30
FF
GG
HH
II
JJ
P41
KK
LL
MM
NN
25 µm
OO
OMP
PP
Kv1.3
QQ
DAPI
RR
MCL
EPL
GL
WT
SS
100 µm
MCL
EPL
GL
Kv1.3 -/-
TT
Kv1.3
55-66 kDa
G olf
52 kDa
β-actin
42 kDa
HEK
P1
P4
P7
P11
P14
P17
P21
P28
>1yr

Figure 1

number of OMP-positive, MOR28-negative axons (Fig. 5V–X,AA).

Collectively, these data are the first to demonstrate that voltage-gated activity, in addition to odor-sensory deprivation (Zou et al., 2004) or odor environment (Kerr and Belluscio, 2006), might modulate homogeneous glomerular development, to alter what was previously hypothesized to be invariant projections from a single class of ORs (i.e., defining the topographic map of odorant information).

Number of projections in Kv1.3-null mice

In the genetically-modified mice, both the P2 and M72 loci encode a bicistronic mRNA (Mountford and Smith, 1995) that allows for translation of the respective ORs along with tau-lacZ (Callahan and Thomas, 1994), which is a fusion of the microtubule-associated protein tau with β-galactosidase (Mombaerts et al., 1996). The ORs are expected to be properly trafficked to the plasma membrane, whereas the soluble β-galactosidase product is cytoplasmic and would be transported down the axons. Presumably, the intensity of the blue precipitated product would reflect the total number of axonal projections and the relative number of sensory neurons expressing P2 or M72 ORs in the epithelium. Qualitatively, the intensity of the β-galactosidase product in both KvP2 and KvM72 was consistently reduced over that observed in respective wild-type whole-mount preparations (Fig. 2). Because we discovered that the concentration of Mg^{2+} induced variability in the staining, careful attention to treating both genotypes with identical batches of histological solutions was made, yet the intensity differences were still apparent. To quantify this observation, P20 aged WTM72 and KvM72 were decalcified, cryoprotected, coronally sectioned, and then processed for β-galactosidase staining by using a neutral red counterstain to image the structural features of the olfactory bulb neural lamina.

There were far fewer axonal projections from M72 expressing OSNs to the OB of KvM72 mice compared with those observed in WTM72 mice, as shown in the representative photomicrographs in Figure 6A,B. The size of the projection in terms of glomerular cross-sectional area was also smaller in the KvM72 mice (Fig. 6E,F) compared with that of WTM72 mice (Fig. 6C,D) for both the lateral and medial M72 glomeruli (significantly different Student's t-test, $p \leq 0.05$, n = 6–11; Fig. 6G). A similar analysis comparing the cross-sectional area of the P2 glomerulus in WTP2 vs. KvP2 animals found that the lateral P2 glomerulus was significantly smaller in the KvP2 animals but that there was no difference in size for the medial P2 glomerulus (Student's t-test, $p \leq 0.05$, n = 6–17; Fig. 6H).

Number of P2-, M72-, and MOR28-expressing OSNS in Kv1.3-null mice

While analyzing the whole-mount preparations (Fig. 2), we noticed that the intensity of the β-galactosidase stain was also reduced in the main olfactory epithelium of the KvM72 and KvP2 mice compared with respective wild-type whole-mount preparations. A higher magnification of the epithelium is shown in Figure 7A,B. To quantify the number of P2 and M72 OSNs in the Kv1.3-deficient background, 16-μm serial sections of nasal epithelium for five mice of each genotype (WTM72, KvM72, WTP2, KvP2) at postnatal day 20 were histologically prepared as frozen sections and processed as in Figure 6. Manual counts of β-galactosidase-positive neurons were made across the entire epithelium of 20 animals, as reported in Figure 7C. There were significantly fewer OSNs expressing P2 or M72 ORs in the $Kv1.3^{-/-}$ background (Student's t-test, $p \leq 0.05$; Fig. 7C), suggesting that loss of voltage-gated activity in mitral cells alters the number of corresponding presynaptic neurons at the periphery. Similar results were obtained for OSNs expressing MOR28 OR (Fig. 7D). Due to the lack of genetic marker, OSNs expressing MOR28 were quantified from serial sections of nasal epithelium immunolabeled with αMOR28. To conserve antiserum, the total number of MOR28-immunoreactive OSNs was counted from every fifth section collected from five P20 aged mice from each genotype (total of 20 sections). The sum number of MOR28-immunoreactive neurons in sampled epithelia from combined identical regions was fewer in the $Kv1.3^{-/-}$ animals than that counted in aged-matched wild-type animals (wild type = 399 ± 49, n = 5; $Kv1.3^{-/-}$ = 319 ± 33, n = 5; significantly different Student's t-test, $p \leq 0.05$; Fig. 7D).

A representative photomicrograph of labeled MOR28 OSNs in wild-type and $Kv1.3^{-/-}$ mice indicated that

Fig. 1. Lack of Kv1.3 ion channel protein expression in the main olfactory epithelium (MOE) by two different immunodetection approaches. **A–NN:** Representative photomicrographs of 16-μm coronal cryosections of the sensory epithelium processed for αKv1.3 (1:500) and α-G_{olf} (1:500) immunoreactivity over a series of postnatal stages at high magnification. P1–P41, postnatal (P) days; NP, no primary control. Representative for P41. Column 1 (G_{olf}), red channel; column 2 (Kv1.3), green channel; column 3 (DAPI, nuclear stain), blue channel; column 4 (DIC [differential interference contrast]), brightfield image; column 5 (merge), overlay of A–D, respectively. Wild-type B6C57 mice (OR untagged mice). **OO–SS:** Representative photomicrographs as above but processed for αKv1.3 (1:500) and/or αOMP (1:1,000) immunoreactivity at lower magnification to be inclusive of other cell types in the epithelium (OO–QQ) or the olfactory bulb (RR–SS). OO–QQ: Note absence of detection of Kv1.3 protein (green channel) but positive immunolabeling for another marker known to detect mature olfactory neurons (OMP; red channel) and axonal processes in the MOE. RR–SS: αOMP immunoreactivity (red channel; converted magenta) is intertwined but non-overlapping with the αKv1.3 signal in the glomerular layer (GL). Arrow, mitral cell body and processes labeled with αKv1.3; **Inset:** Higher magnification of mitral cell layer (MCL) and associated processes. Note positive immunolabeling for Kv1.3 protein in the olfactory bulb of wild-type B6C57 mice (WT) but absence of detection in mice with Kv1.3-gene-targeted deletion ($Kv1.3^{-/-}$). EPL, external plexiform layer. Postnatal day 41. **TT:** Representative Western blot in which 25 μg of purified epithelial membrane proteins were separated by SDS-PAGE and electro-transferred to nitrocellulose for wild-type B6C57 mice. Proteins were harvested at various postnatal stages as noted. Nitrocellulose was blotted with a polyclonal antibody against Kv1.3 (αKv1.3; 1:1,000) with M_r = 55–66 kDa (depending on phosphorylation state) and then stripped and reprobed with anti-β-actin (α-β-actin; 1:1,000) to confirm equal loading of protein. Cloned Kv1.3 channel protein, heterologously expressed in HEK293 cells (HEK) and prepared as a cell lysate, was used as a positive migration standard. Labeling with an antibody to another membrane-bound protein (α-G_{olf}; 1:1,000) known to be enriched in MOE membranes was used as an additional positive control. Scale bar = 25 μm in NN (applies to A–NN) 100 μm in SS (applies to OO–SS); 10 μm in inset to RR.

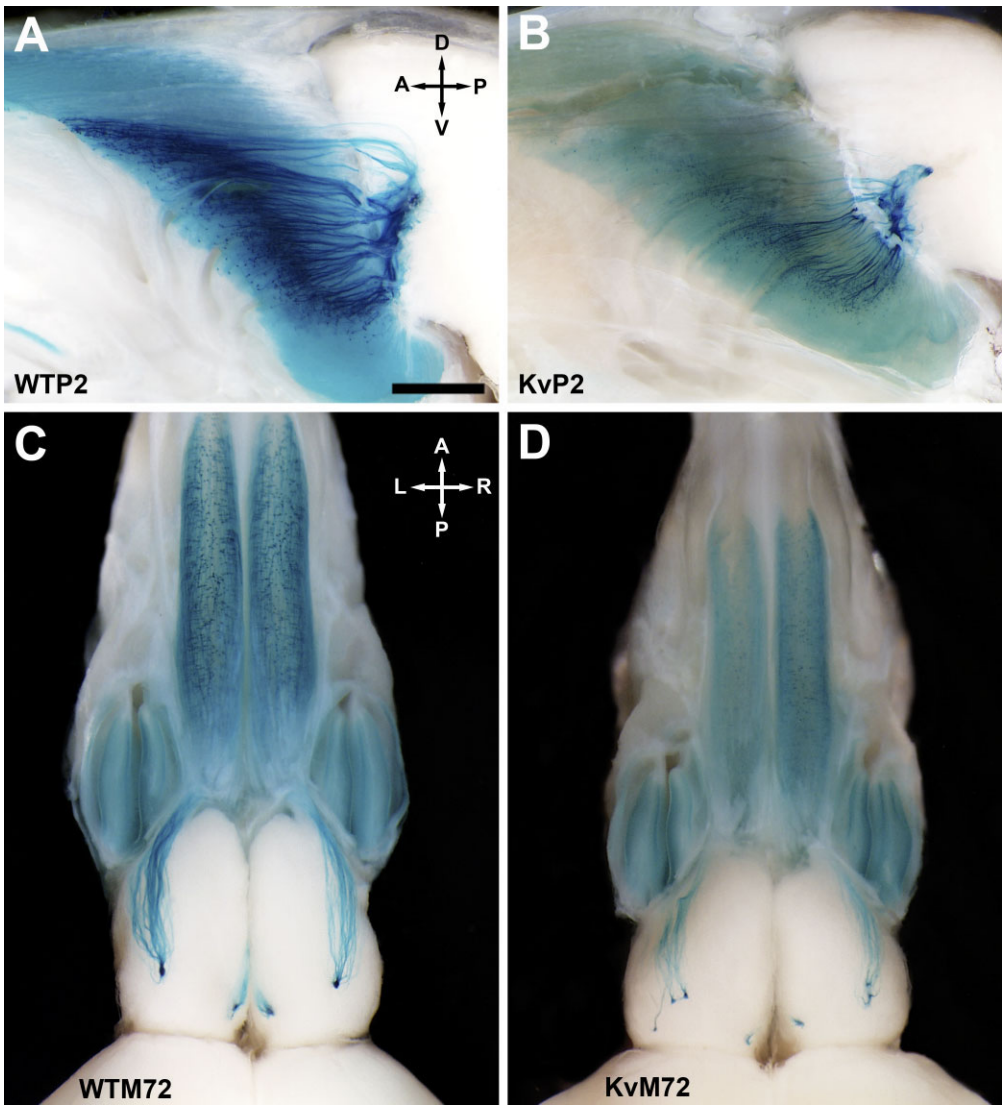

Fig. 2. Axonal projections from P2- and M72-expressing olfactory sensory neurons (OSNs) to the olfactory bulb of wild-type and Kv1.3-null mice. **A:** Representative whole-mount photograph of the olfactory bulb of a P2-IRES-tau-LacZ (WTP2) mouse at postnatal day 20 (P20). Axonal projections from olfactory sensory neurons (OSNs) expressing the odorant receptor P2 were visualized by histological staining for β-galactosidase that was created as a fusion protein with tau immediately downstream of the P2 odorant receptor stop codon (Mombaerts et al., 1996). Brain whole-mounts were viewed through a Leica MX FLIII stereomicroscope, and images were captured with an Olympus DP10 digital camera. A, anterior; D, dorsal; P, posterior; V, ventral. **B:** Same as A but for a Kv1.3-null P2-IRES-tau-LacZ double-homozygous mutant mouse (KvP2). Note reduction in total β-galactosidase intensity in comparison with that of wild-type mice (A). **C:** Same as A but for an M72-IRES-tau-lac-LacZ (WTM72) mouse. A, anterior; L, left; P, posterior; R, right. **D:** Same as C but for a Kv1.3-null M72-IRES-tau-LacZ double-homozygous mutant mouse (KvM72). The glomerular projections are supernumerary, as is particularly apparent in the lateral side. Note also the moderate reduction in both olfactory bulb and epithelial size (for brain/body weight ratios, see text). Similar to that observed for KvP2 mice (B), note the reduction in total β-galactosidase intensity. Scale bar = 1 mm in A (applies to A–D).

whereas there was a reduction in total number of OSNs in the Kv1.3$^{-/-}$ background, interestingly, there was a sizable increase in MOR28 labeling at the cilia (Fig. 7E,F). Some of the micrographs also indicated that the soma of the MOR28 OSNs in Kv1.3$^{-/-}$ might be higher in the epithelium, but this slight change in position did not reach statistical significance (depth of soma = 32.8 ± 1.9 μm (wild type) vs. 29.7 ± 1.5 μm (Kv1.3$^{-/-}$), not significantly different by Student's *t*-test, $p > 0.05$, n = 17). Changes in OR expression have been reported to affect either targeting or the zonal organization within the epithelium (Feinstein et al., 2004; Feinstein and Mombaerts, 2004); thus we also wondered whether the pattern of expression for these receptors was consistent with that observed in wild-type mice or whether the altered subcellular distribution of MOR28 created altered zonal distribution patterns in the epithelium.

As shown in representative sections in Figure 7G–J, we observed that whereas the total number of M72-expressing OSNs was fewer in the Kv1.3-null back-

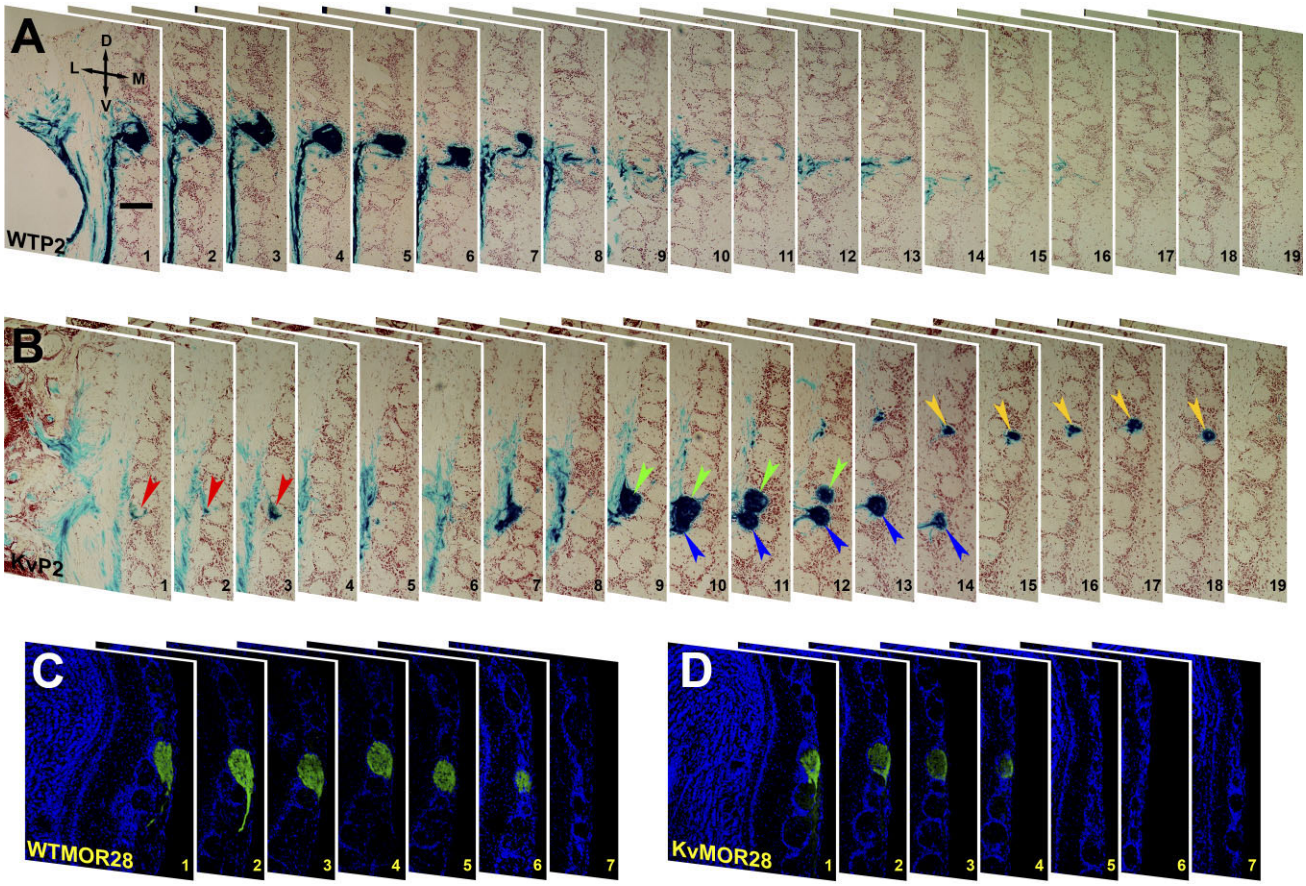

Fig. 3. Axonal projections from P2- and MOR28-expressing OSNs to the OB of wild-type and $Kv^{-/-}$ mice. **A:** Photomicrographs of 16-μm serial coronal cryosections of the OB of a P2-IRES-tau-LacZ (WTP2) mouse at P20 showing the lateral glomerulus. Sections were processed for β-galactosidase histochemistry and then counterstained with neutral red to delineate P2 axonal projections. Note the presence of a single glomerulus that is seen across sections 1–7. Section 1 is the anterior, and section 19 is the posterior. D, dorsal; L, lateral; M, medial; V, ventral. **B:** Same as A but for a Kv1.3-null P2-IRES-tau-LacZ double-homozygous mutant mouse (KvP2). Note the presence of four different glomeruli (color-coded arrowheads) seen across sections 1–19. **C:** Photomicrographs of 30-μm serial coronal cryosections of the OB of an OR untagged wild-type mouse (WTMOR28) at P20. Sections were first immunolabeled with αMOR28 to delineate the MOR28 glomerulus and then counterstained with DAPI. Orientation is the same as in A. **D:** Same as C but for an OR untagged $Kv1.3^{-/-}$ mouse (KvMOR28). Unlike KvP2 (B), no extra MOR28 glomeruli were present in $Kv1.3^{-/-}$ mice. Scale bar = 75 μm in A (applies to A–D).

ground, the pattern of zonal expression did not appear to be altered. Similar results were obtained with P2 and MOR28 OSNs in terms of unchanged zonal OR expression pattern (data not shown). Alternatively, we questioned whether the observed increase in OR expression at the cilia was partially attributed to a changed morphology of the OSNs of $Kv1.3^{-/-}$ mice. Upon closer examination of wild-type and $Kv1.3^{-/-}$ OSNs at age P20 by scanning electron microscopy (SEM), it appeared that the density of individual OSNs was less in the Kv1.3-deficient background. These data are consistent with the reduction in OR-specific OSNs counts observed via light microscopy; however, by SEM we could also resolve whether the number of individual cilia per OSN appeared to be increased (Fig. 7K,L). Counts of cilliary rudiments in a small sample of preparations (n = 10) indicated that there were 14.0 ± 0.5 cilia/OSN from wild-type animals vs. 20.0 ± 1.1 cilia/OSN from $Kv1.3^{-/-}$ animals (significantly different by Student's *t*-test, $p \leq 0.05$). Each preparation represented a field of view of approximately 15 neurons with preparations made from at least three different animals per genotype. A full ultrastructural analysis would be warranted to quantify our initial observations; however, this type of structural arrangement would certainly support increased OR expression at the cilia as well as a supersmeller behavioral phenotype (Fadool et al., 2004).

Olfactory receptor and G_{olf} expression levels are altered in $Kv1.3^{-/-}$ mice

Our histological data show that the expression of three different OR-specific OSNs was clearly downregulated in the absence of Kv1.3 ion channel, but one could question whether lack of voltage-gated activity affects the expression of ORs and peripheral transduction proteins more globally. To test this hypothesis, we probed purified membrane preparations of nasal epithelium with three different antisera (αOR256-17, αMOR28, and αMOR50) directed to unrelated (different subfamilies) odorant receptor proteins in OR-untagged wild-type and $Kv1.3^{-/-}$

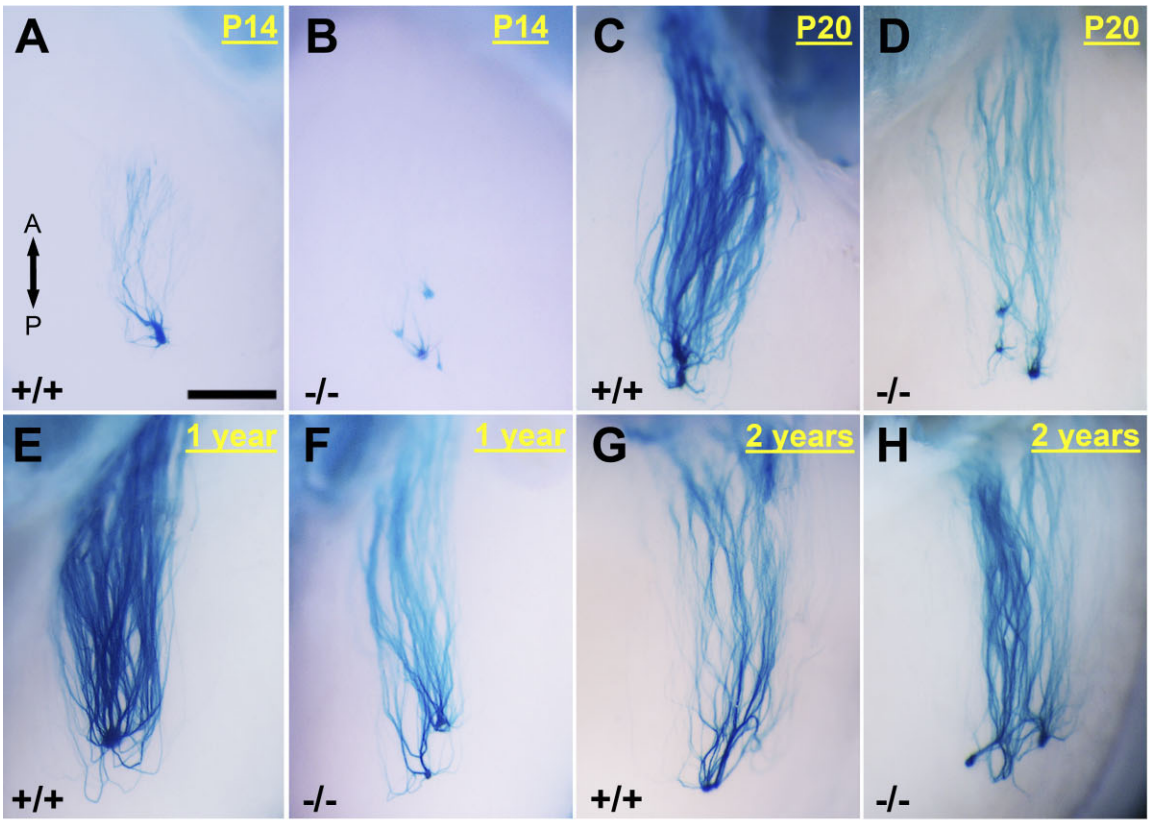

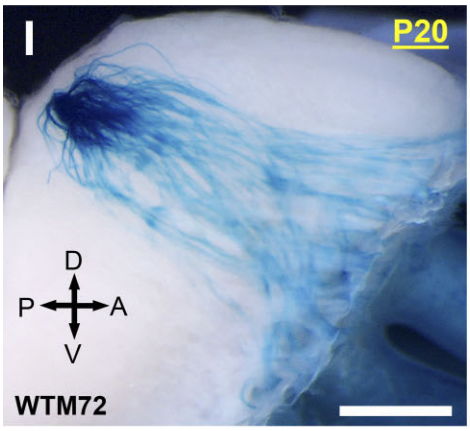

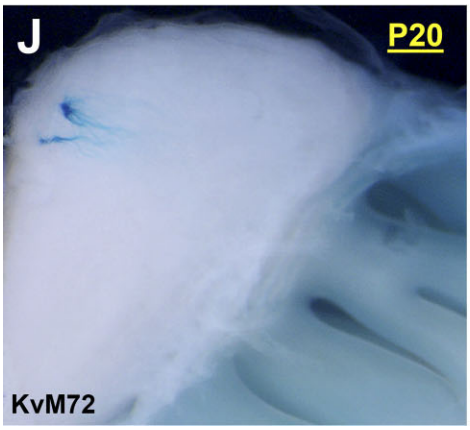

K

	Age (n)	Glomeruli/Bulb (Min-Max)
WTM72	P8-10 (4)	2.25 (2-3)
	P20 (10)	2.4 (2-3)
	P30 (4)	2.75 (2-3)
	P>1year (5)	2.25 (2-3)
KvM72	P8-10 (10)	4.3 (3-6)
	P20 (28)	4.17 (3-7)
	P30 (4)	4.25 (4-5)
	P>1year (3)	4.00 (4-4)

L

	Age (n)	Glomeruli/Bulb (Min-Max)
WTP2	P20 (5)	3.1 (2-4)
	2 years (2)	5.5 (5-6)
KvP2	P20 (5)	5.0 (4-6)
	2 years (3)	7.83 (6-10)

Fig. 4. Supernumerary axonal projections from M72- and P2-expressing OSNs of KvM72 and KvP2 mice are independent of developmental age. **A–H:** Representative whole-mount photographs prepared and captured as in Figure 2 for M72-IRES-tau-LacZ (+/+) and Kv1.3-null M72-IRES-tau-LacZ (−/−) mice taken at various postnatal (P) ages from 14 days to 2 years. These photographs were taken at higher magnification for the lateral projection only. A, anterior; P, posterior. **I–J:** Same as A–H but for the medial projection at P20. Number of M72 axons and the size of glomeruli were dramatically reduced in KvM72. Orientation abbreviations as in Figure 2. **K:** Summary of the mean number of M72 glomeruli observed (range in parentheses) in WTM72 versus KvM72 mice as reported for various developmental ages. **L:** Same as K but for WTP2 and KvP2 mice. Scale bar = 0.5 mm in A (applies to A–H); 1 mm in I (applies to I,J).

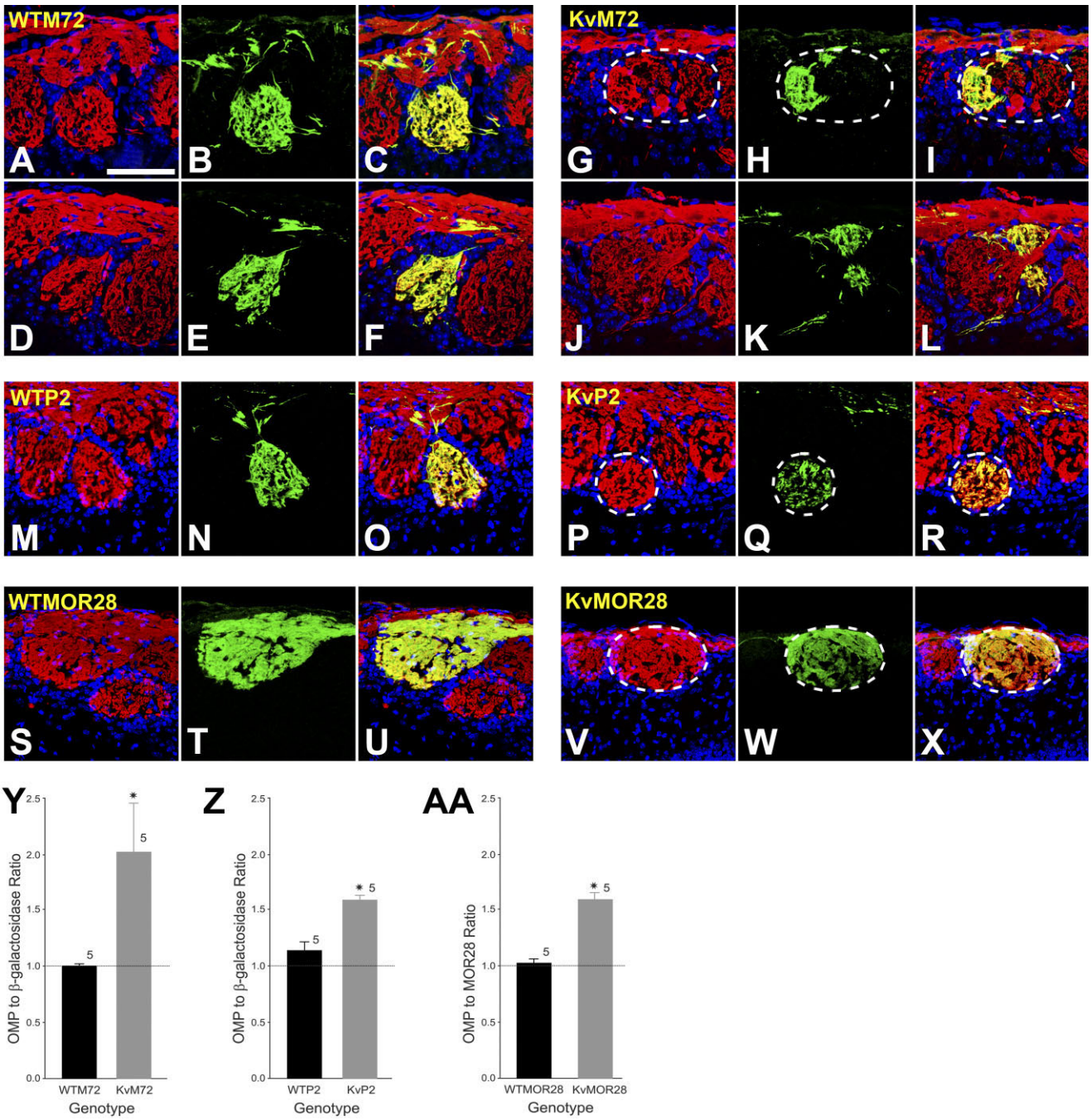

Fig. 5. Absence of Kv1.3 ion channel induces the development of heterogeneous glomeruli. **A–L:** Representative two-photon confocal micrographs of WTM72 (left panels; A–F) and KvM72 glomeruli (right panels; G–L). A,D,G,J: Red channel; sections were processed for olfactory marker protein (OMP; 1:1,000) immunocytochemistry to visualize axons projecting from all mature OSNs. B,E,H,K: Green channel; sections were processed for β-galactosidase immunocytochemistry (1:1,000). C,F,I,L: Merged image, yellow. Note the incomplete innervation of the M72 glomerulus (I,L) in KvM72 as evidenced by red only fibers creating a heterogeneous M72 glomerulus. Postnatal day 20. **M–R:** Representative two-photon confocal micrograph of a WTP2 (M–O) and a KvP2 glomerulus (P–R). Red channel represents OMP; green, β-galactosidase; yellow, merged image. Note the presence of a heterogeneous P2 glomerulus (R) in the KvP2 mouse. A few OMP-positive, β-galactosidase-negative fibers are also visible in WTP2 mice (O). **S–X:** Representative two-photon confocal micrograph of a WTMOR28 (S–U) and a KvMOR28 glomerulus (V–X). Red channel represents OMP; green, MOR28 immunoreactivity; yellow, merged image. KvMOR28 mice exhibit heterogeneous glomeruli (X). **Y:** Histogram plot of αOMP to α-β-galactosidase pixel density for M72 glomeruli of WTM72 and KvM72 mice. A ratio of 1.0 represents complete overlapping of OMP and β-galactosidase-immunoreactive axons (homogeneous glomerulus), whereas a ratio > 1.0 represents more OMP-immunoreactive axons (heterogeneous glomeruli). Values are mean ± SEM. *, significantly different by Student's *t*-test, $p \leq 0.05$. **Z:** Same as Y but for WTP2 and KvP2. **AA:** Histogram plot of αOMP to αMOR28 pixel density for MOR28 glomeruli of WTMOR28 vs. KvMOR28 mice. Values are mean ± SEM. *, significantly different by Student's *t*-test, $p \leq 0.05$. Scale bar = 100 μm in A (applies to A–X).

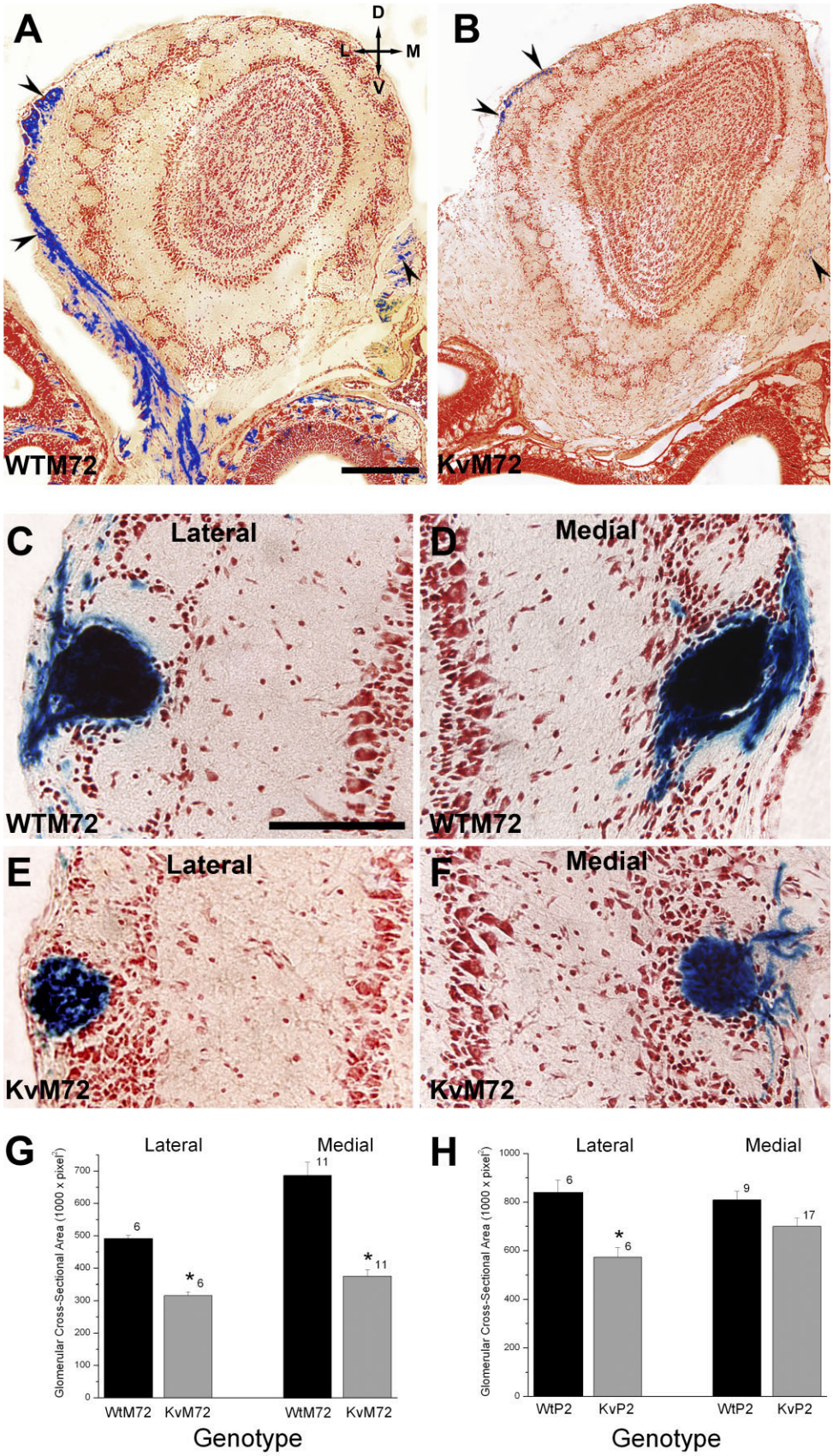

Fig. 6. Total number of axon projections and the size of the P2 or M72 glomerulus is reduced in the absence of Kv1.3 channel. **A,B:** Representative photomicrographs of 16-μm coronal cryosections processed to visualize β-galactosidase to delineate the axons (arrowheads) from OSNs expressing M72 at postnatal day 20. Sections were counterstained with neutral red. Left, WTM72; right, KvM72. **C–F:** Same as A but higher magnification of the M72 lateral (Lateral) and medial (Medial) glomerulus of a representative WTM72 (C–D) vs. KvM72 (E–F) mouse. **G:** Histogram plot of the glomerular cross-sectional area of the M72 lateral and medial glomerulus in a population of WTM72 vs. KvM72 mice. Values are mean ± SEM number of glomeruli measured for at least six mice for each genotype. *, significantly different by Student's *t*-test, $p \leq 0.05$. **H:** Same as G but for the P2 glomerulus in WTP2 vs. KvP2 mice. Scale bar = 250 μm in A (applies to A,B); 100 μm in C (applies to C–F).

mice (Fig. 8A–C). Two of the antisera (αOR256-17 and αMOR50) were generous gifts from other investigators with characterized specificity in epithelial sections (Barnea et al., 2004; Strotmann et al., 2004) but untested antigenicity for denatured conditions.

The third OR probe (αMOR-28) was a pair of antisera with previously reported antigenicity in sections and via Western blotting, respectively (Barnea et al., 2004). Quantification of OR densitometry had to be restricted to MOR28 and MOR256-17 (Fig. 8A,B) by Western blot analysis due to nonspecific labeling with MOR50. Specific labeling of both αMOR28 and αMOR256-17 at their predicted MW (35.4 kDa/36.8 kDa; Protein Param Program, ExPASy, http://us.expasy.org/cgi-bin/protparam) was significantly increased in purified epithelial membranes prepared from Kv1.3$^{-/-}$ mice compared with that prepared from wild-type mice (Fig. 8C).

We hypothesized that if the majority of OR, if not all, are upregulated in Kv1.3$^{-/-}$ mice, we should observe an increase in the level of G_{olf} in the cilia of OSNs. Frozen sections of nasal epithelia of receptor untagged wild-type and Kv1.3$^{-/-}$ mice were immunostained with G_{olf} antiserum. Areas of the nasal epithelium representing ectoturbinate I, ectoturbinate II, and endoturbinate II are shown in Figure 8D–I. These areas were selected because they collectively represent all four zones of the nasal epithelium. Qualitative and quantitative analyses showed a sizable increase in G_{olf} immunoreactivity at the cilia of Kv1.3$^{-/-}$ compared with that of wild-type mice (wild type: 47.6 ± 2, n = 5; Kv1.3$^{-/-}$: 80.1 ± 1.2, n = 5; significantly different by Student's *t*-test, $p \leq 0.05$; Fig. 8J).

DISCUSSION

Three generic models have been proposed to explain how ORs might function in axonal guidance: 1) ORs might interpret positional information in the olfactory bulb; 2) ORs might utilize odorant transduction and information of correlated patterns of odorant-evoked activity; and 3) ORs might utilize molecular interactions across axons (Feinstein and Mombaerts, 2004). Interestingly, none of these models employ voltage-activated processes or even show how neural activity might modulate the coding of olfactory information to provide a degree of plasticity that is inherently required of most sensory systems (e.g., the visual system; LeVay et al., 1980). Through traditional loss of function approaches using gene-targeted deletion combined with genetically-tagged OR mouse models, we are now able to demonstrate that voltage-gated activity in the olfactory bulb 1) prevents heterogeneous glomerular development in which there could be mixed synaptic loci between axons of unlike OR proteins; 2) helps to refine and stabilize the axonal projection initially defined by OR sequence identity and regulated by guidance molecules (without it, extranumerary glomeruli may develop); and 3) modulates the number of OSNs at the periphery (without it, OR and G-protein expression is compensatorily increased).

Certainly action potential spike generation in olfactory sensory neurons that is propagated to mapped central targets is both shaped by chemical (odorant) evoked activity and modulated by voltage-gated activity (Yu et al., 2004). This is the first report demonstrating that centrally derived, voltage-gated activity alters refinement of connections to central targets and simultaneously reduces peripheral OSNs. In other loss of function studies, two key olfactory signal transduction proteins, the CNG channel and the G-protein G_{olf}, were not required for generating synaptic specificity in the olfactory bulb (Belluscio et al., 1998; Lin et al., 2000). In the CNG-null animals, the interpretation that odorant-evoked activity does not influence axonal projections is somewhat muddled by the new finding that these mice are not completely anosmic, as initially reported (Brunet et al., 1996), and respond behaviorally (olfactometer), electrically (electro-oculography [EOG]), and cellularly (cfos activity) quite well to odorants that are classified as pheromone-like compounds (heptanone and 2,3-dimethylpyrazine [DMP]; Lin et al., 2006, 2007).

In addition, recent genetic manipulation of stimulatory G protein has demonstrated that cAMP may regulate the expression of axon guidance molecules essential for OR-instructed axonal projections (Imai et al., 2006). Unfortunately, the behavioral phenotype of these mice, with a point mutation in the conserved tripeptide motif for coupling G proteins, was not reported, nor was any characterization of spontaneous spike generation. Although OMP is not classified as a signal transduction protein per se, loss of OMP in OSNs causes an overshooting of sensory axons into the external plexiform layer, which persists in mice up to 8 months of age (St. John and Key, 2005). Because mice with gene-targeted deletion of OMP have altered OSN electrophysiological function and an altered behavioral response to odorant stimulation (Buiakova et al., 1996; Youngentob and Margolis, 1999; Youngentob et al., 2001), it is an interesting parallel that Kv1.3-null animals (altered OB electrophysiological function and enhanced behavioral discrimination of odorants) also demonstrate fixed (up to 2 years) synaptic mistargeting in the form of supernumerary glomerular connections.

How might mitral cell activity modulate the refinement of presynaptic OSNs? In other sensory systems, synapse formation is initially achieved by genetically determined cues, but subsequent refinement requires spontaneous neural activity and sensory experience (Katz and Shatz, 1996). In the visual system, refinement of the topographic map is thought to require the participation of postsynaptic cells, such that correlated activity in presynaptic neurons results in the release of factors that subsequently modify the presynaptic arbors (Cramer and Sur, 1995; Fitzsimonds and Poo, 1998). In particular, blockade of the *N*-methyl-D-aspartate (NMDA) receptor that alters activity of postsynaptic cells significantly influences the patterning of inputs and the structure of presynaptic afferents in the visual system (Hahm et al., 1999). It might be possible that a similar mechanism may exist in the olfactory system to refine the glomeruli toward a homogeneous entity of similar axons. In a recent report by Guthrie and co-workers (Ardiles et al., 2007), focal NMDA-induced ablation of postsynaptic neurons in the olfactory bulb caused disruption of new axon targeting to P2 glomeruli. In their study, elimination of synaptic contacts did not cause axons within previously established glomeruli to wander, rather, *new* P2 axons coalesced at inappropriate locations and formed smaller glomeruli. Thus our results and those of Ardiles et al. (2007) provide support for the notion that OB map stability and its continual refinement relies on a normal distribution or function of synaptic targets, such as mitral cell neurons, in the olfactory bulb.

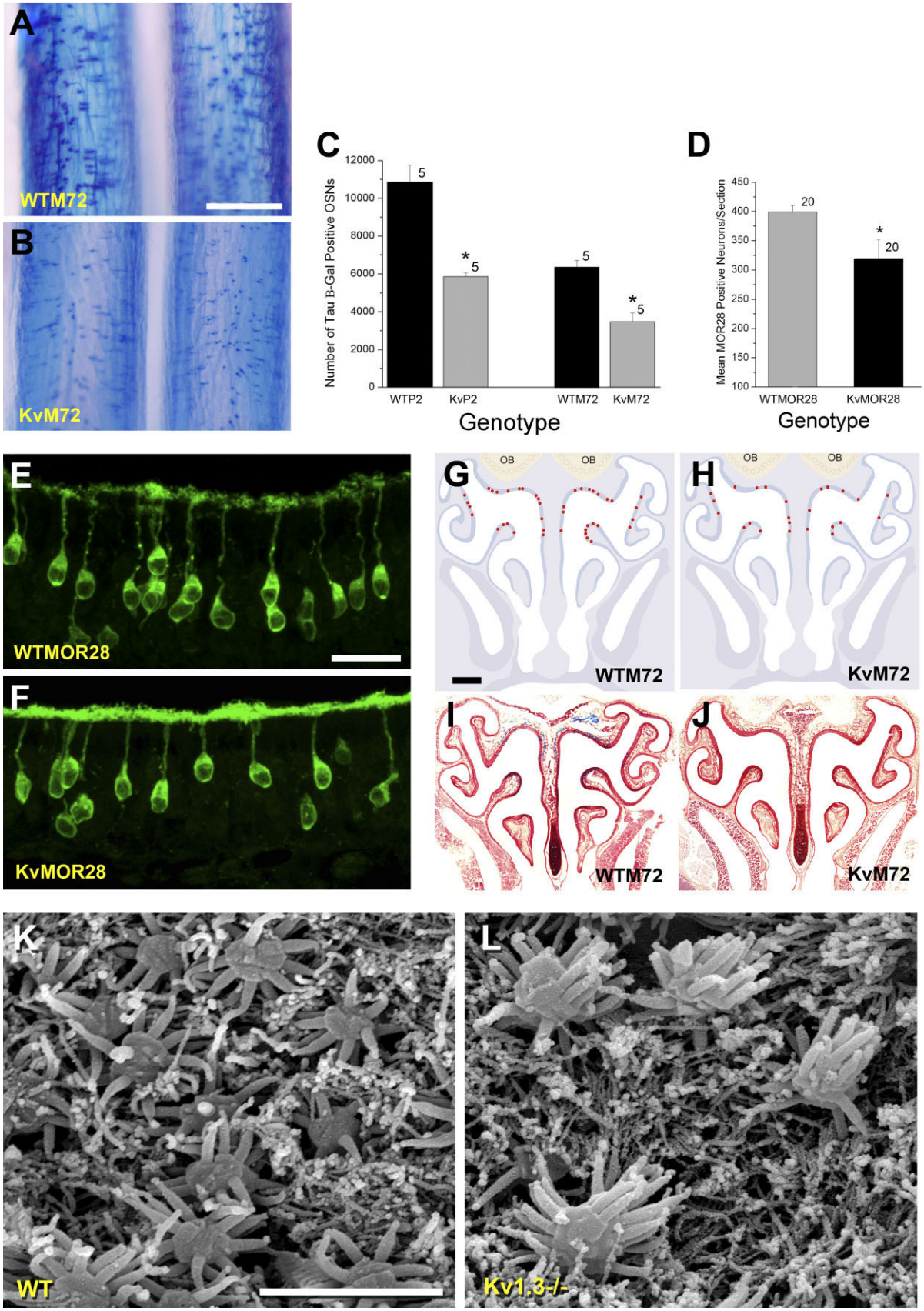
A
WTM72
B
KvM72
C
Number of Tau ß-Gal Positive OSNs
12000
10000
8000
6000
4000
2000
0
5
*5
5
*5
WTP2
KvP2
WTM72
KvM72
Genotype
D
Mean MOR28 Positive Neurons/Section
450
400
350
300
250
200
150
100
20
*20
WTMOR28
KvMOR28
Genotype
E
WTMOR28
F
KvMOR28
G
OB
OB
WTM72
H
OB
OB
KvM72
I
WTM72
J
KvM72
K
WT
L
Kv1.3-/-

Figure 7

Axel and co-workers (Yu et al., 2004) suggest that spontaneous neural activity but not odor-evoked activity is required for both the maintenance and precise connectivity inherent in the olfactory sensory map. In a recent report, they engineered overexpression of a different potassium channel, the inward-rectifying potassium channel (Kir2.1), and although this channel is not known to be natively expressed in the olfactory system (Doupnik et al., 1995), the design was to decrease excitability of OSNs via hyperpolarization, which they discovered severely disrupted the formation of the sensory map (Yu et al., 2004). This study, in combination with our current report, provides good comparisons to increase our knowledge of the role of voltage-gated activity in the encoding of olfactory information. The hyperpolarization driven by overexpression of Kir2.1 at the periphery and increased excitability of mitral cells evoked by deletion of Kv1.3 centrally can thus both drive changes in axonal connectivity even though they are opposite electrical events. The changes, however, appear to be OR-type dependent, in that Kir2.1-mediated silencing of OSNs caused an increase in P2 glomerular targeting (up to 16 innervations) whereas Kv1.3 deletion increasing mitral cell excitability caused a two- to three-fold increase in both P2 and M72 projections but no change in MOR28 projections.

The defect in axon targeting created by both potassium channel alterations was associated with a decrease in OSN expression and/or changes in epithelial patterns of expression even though one mutation elicited mitral cell excitability and the other a depression in OSN spontaneous activity. Because we cannot detect expression of Kv1.3 in the main olfactory epithelium by either SDS-PAGE or immunocytochemistry (Fig. 6) and because expression is predominantly, but not exclusively, localized to the mitral cells (Fadool et al., 2000; Colley et al., 2007, Marks and Fadool, 2007), the increased frequency of action potential firing centrally in the olfactory bulb may be modulating OR protein expression, as well as altering typically singular axonal projections to be supernumerary, the latter of which appear to be OR-type dependent. An alternative hypothesis, which our data cannot eliminate, is that deletion of Kv1.3 may be affecting electrical events at even higher areas of olfactory processing in the piriform cortex (Kues and Wunder, 1992; Colley et al., 2007) or events in the dentate gyrus of the hippocampus (Kues and Wunder, 1992) or the hypothalamus (Tucker et al., 2007). Whether higher order CNS neurons are also affected by Kv1.3 deletion must be explored; however, our data and those reported by a large microarray survey of 10,000 genes contained in OMP/gfp$^+$ cells of the MOE (Sammeta et al., 2007) make it unlikely that *Shaker* family members drive voltage-gated activity in OSNs at the periphery because the gene and the protein are not expressed.

Kv1.3-null mice have both anatomical alterations as well as electrical changes that could underlie their increased olfactory ability for odor threshold and discrimination. Because we found fewer OSNs in the Kv-null condition for our subsets (P2, M72, MOR28), each apparently expressing a greater density of OR proteins, combined with the greatly reduced number of total axonal projections (despite their supernumerary synaptic connections), we suggest that this might provide a different convergence of information in the "supersmeller" animal. We have noted that whereas the threshold odorant concentration detected by these animals is 10,000 times less than that of wild-type animals, the Kv-null animals take longer intervals to make this decision, especially at higher odorant concentrations (Fadool et al., 2004). Anatomically, this may be aligned with a reduced convergence of axons to a defined glomerulus (fewer OSNs and concomitant projections; Figs. 6,7) and a greater pattern of divergence once the OB has been reached (more mitral cells in Kv-null animals; Hoffman and Fadool, unpublished data).

Our data suggest that altered voltage-gated activity does not grossly perturb the projection of axons from OSNs to the glomerular target but rather disrupts the refinement by creating supernumerary synaptic connections. In fact, convergence of P2 axons has been demonstrated to be completely independent of the presence of the OB (St. John et al., 2003), but the refinement of these synaptic connections once they have arrived at the OB is what is perturbed without Kv1.3. Implantation, organotypic co-cultures, and organ ablation studies collectively support a dynamic development of the combined olfactory epithelium and the laminar organization of the olfactory bulb (Graziadei et al., 1978, 1979; Storan and Key, 2004; Chehrehasa et al., 2006). At the same time, each organ can develop independently in vivo or in vitro in the absence of normal pathfinding cues. For example, OSNs can fasciculate or even regenerate following complete surgical bulbectomy or in mouse genetic models that lack the OB or lack interactions between the OB and OE, and they can also project into foreign target tissues (Graziadei et al., 1978; Long et al., 2003; St. John et al., 2003; Storan and Key, 2004). In contrast, peripheral genetic ablation of the MOE can cause the misorientation of mitral cell dendrites (López-Mascaraque et al., 2005). We conjecture that

Fig. 7. Absence of Kv1.3 ion channel decreases the number of M72-, P2-, and MOR28-expressing OSNs in the epithelium. **A,B:** Representative photomicrographs of whole-mount processed epithelium (as in Fig. 2) to visualize M72-expressing OSNs in WTM72 vs. KvM72 mice. Note fewer tau β-galactosidase-positive neurons in the KvM72 mice (B). Postnatal day 20. **C:** Histogram plot of the number of tau β-galactosidase-positive OSNs manually counted through entire epithelium prepared as 16-μm serial sections plotted against genotype. Postnatal day 20. Genotype abbreviations as in Figure 1. Values are mean ± SEM. Sample size is number of whole epithelia (mice). *, significantly different by Student's *t*-test, $p \leq 0.05$. **D:** Histogram plot of the number of MOR28-immunopositive OSNs as described in text. Each bar represents the mean number (± SEM) of OSNs in 20 sections. *, significantly different by Student's *t*-test, $p \leq 0.05$. **E,F:** Higher magnification light photomicrograph (63× oil) of OSNs processed for MOR28 immunocytochemistry in wild-type (WT-MOR28) and Kv1.3$^{-/-}$ (KvMOR28) mice. In this and subsequent panels of Figure 8, laser gain and offset intensity were set to that of control sections treated by incubating with similar solutions but lacking the primary antiserum. NIH Image J was used to quantify pixel intensity in identical 100-μm cilia regions as compared across genotypes (reported in the text). To conserve antiserum, every fifth section was examined (total of 20 sections/animal) across five animals per genotype. Postnatal day 20. **G–J:** Diagrammatic sketch of M72 OR expression patterns in the epithelium of WTM72 and KvM72 mice. Representative sections processed for the presence of β-galactosidase-positive OSNs are shown in the bottom panels. **K,L:** Scanning electron micrograph of representative olfactory epithelia of receptor untagged wild-type (WT) and Kv1.3$^{-/-}$ mice. As in the light microscopy images (A,B,E,F), the number of OSNs is decreased in Kv1.3$^{-/-}$ mice; however, individual OSNs show an increased number of cilia compared with those of wild-type mice, which is resolved at the ultrastructural level. Scale bar = 500 μm in A (applies to A,B); 25 μm in E (applies to E,F); 700 μm in G (applies to G–J); 3 μm in K (applies to K,L).

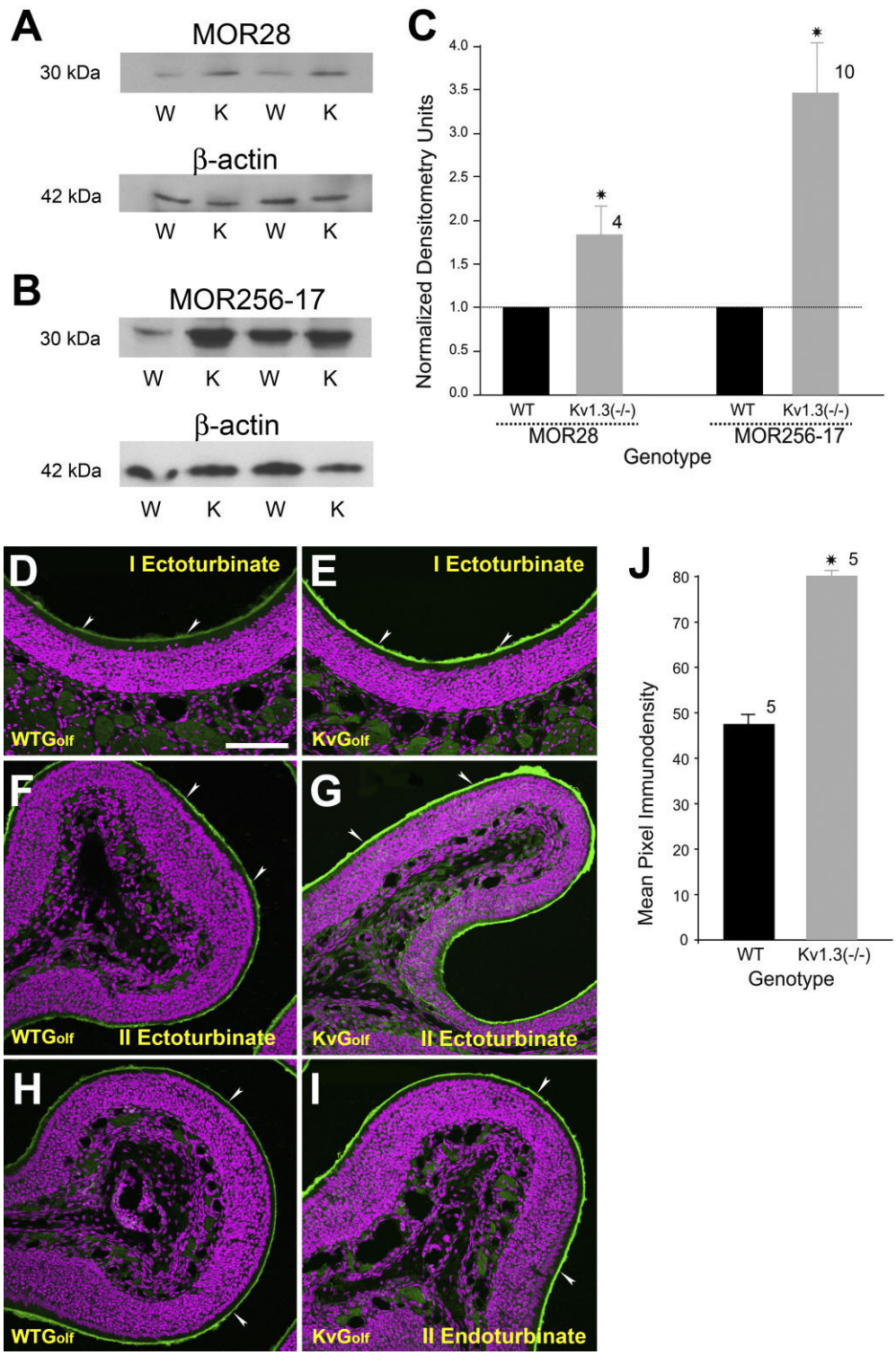

Fig. 8. Olfactory receptor proteins and the G-protein G_{olf} are upregulated in Kv1.3$^{-/-}$ mice. **A,B:** Two representative Western blots in which 30 μg of purified epithelial membrane proteins were separated by SDS-PAGE and electro-transferred to nitrocellulose for two pairs of animals, respectively. Proteins were harvested at P20. Nitrocellulose was blotted with (A) a monoclonal antibody against MOR28 (αMOR28; 1:1,000) or (B) a polyclonal antiserum against mOR256-17 (αMOR256-17; 1:1,000) with a predicted M_r = 35.4/36.8 kDa (ExPASy software, Protein Param, http://us.expasy.org/cgi-bin/protparam) and then stripped and reprobed with anti-β-actin (α-β-actin; 1:1,000) to confirm equal loading of protein. W, wild-type B6C57 mice (OR untagged mice); K, Kv1.3$^{-/-}$ mice. **C:** Histogram plot of the quantitative immunodensity ratios of Kv1.3$^{-/-}$ over wild type for a population of mice normalized within nitrocellulose blot and identical ECL exposure. Dashed line, 1.0 ratio. *, significantly different by Student's *t*-test, Arc-Sin transformation for percentage data, $p \leq 0.05$. **D–I:** Two-photon confocal micrographs of G_{olf} immunoreactivity (arrowheads) in the cilia of OSNs in OR untagged wild-type (WTG_{olf}) and Kv1.3$^{-/-}$ (KvG_{olf}) mice. Note an increase in the intensity of G_{olf} immunoreactivity in KvG_{olf} mice (green channel). Magenta, pseudo-colored DAPI nuclear stain. **J:** Histogram plot of the intensity of G_{olf} immunoreactivity in WTG_{olf} and KvG_{olf} mice (green channel). Quantification and analysis of pixel intensity cilia labeling as in Figure 7E,F. To conserve antiserum, every fifth section was examined (total of 20 sections/animal) across five animals per genotype. Values are mean ± SEM. *, significantly different by Student's *t*-test, $p \leq 0.05$. Scale bar = 100 μm in D (applies to D–I).

whereas loss of Kv channels may perturb the developmental relationship between the MOE and the OB (increased OR expression, reduced number of OSNs, increased abundance of glomeruli), loss of voltage-gated activity perturbs refinement or balance of connections and does not drive large-scale convergence of axons to target terminations.

The alternative view that axons do not converge onto a pre-existing glomerulus structure to serve as a target for axons of OSNs expressing a single OR type but rather coalesce to form a glomerulus driven by OR sequence specificity and homophilic interactions is a strongly supported theory called *contextual axonal sorting* (Feinstein and Mombaerts, 2004; Mombaerts, 2006). Recent experimental evidence suggests that OR-derived cAMP signals, rather than direct action of ORs, determine the OSN axonal projections (Imai et al., 2006). Our data suggest that once axons arrive to congregate into relatively broad regions of the proto-glomerulus, the excitability of the mitral cells may regulate the precision of the projection to retain a homogeneous glomerulus and not one of mixed OSN axonal origins. Whether there is a disruption of expression/maturation of mitral cell neurons (Bulfone et al., 1998) or an alteration of their electrical signaling (action potential firing pattern; Fadool et al., 2004), it is the degree of preciseness in synaptic connection that is altered or the process of neural pruning once the axon arrives at the correct position on the sensory map. With the persistent lack of Kv1.3 activity, the refinement is not merely temporally delayed as it is with glomerular development during naris-occlusion (Nakatani et al., 2003; Zou et al., 2004), but rather the extranumerary synaptic connections are persistent throughout the life of the animal, remaining unpruned.

Alternatively, supernumerary glomeruli created by altered mitral cell activity might be explained by a model of *interdependent interaction* between sensory neurons (Ebrahimi and Chess, 2000). According to this model, after the axons arrive at a particular glomerulus, the presence of additional axons of like OR expression is required to maintain the glomerulus. The theory of interdependence predicts that, if there are only a small number of OSNs expressing a given receptor, then the convergence will not always be maintained. In Kv1.3-null mice there were approximately 50% fewer M72 and P2 OSNs compared with wild type. This might very well explain the presence of extra M72 and P2 glomeruli in Kv1.3-null mice. The MOR28-expressing neurons, however, showed only a 20% reduction in Kv1.3-null mice. Our observation that Kv1.3-null mice lacked extra MOR28 glomeruli might suggest that although this class of OSNs was reduced, there may still have been enough neurons to reach the apparent threshold for activation of the "interdependence interaction" of like MOR28 axons.

Although the numbers of M72, P2, and MOR28 OSNs were dramatically reduced in Kv1.3$^{-/-}$ mice, the intensity of G_{olf} immunoreactivity and OR pixel density (MOR28 and MOR256-17) was significantly greater than that of wild-type mice. Our data do not discern whether the increased G_{olf} and OR immunoreactivity was due to more cilia, as suggested by our SEM data, or to an increase in length of the cilia (or both). The upregulation of G_{olf} and ORs might reflect a compensatory mechanism to balance fewer OSNs in Kv1.3$^{-/-}$ mice. Cell volume changes and the elevated flux of intracellular potassium, which accompanies apoptosis, can contribute to increased activity and expression of Kv1.3 (Szabo et al., 2004). Given the developmental interactions between pre- and postsynaptic targets, in the absence of Kv1.3 in central targets, it is possible that the balance of programmed cell death and regeneration of olfactory synaptic connections is disturbed. It is also conceivable that surviving sensory neurons are those that already express a high level of OR protein and are not undergoing programmed cell death.

Unlike the loss reported by Ardiles et al. (2007), whereby postsynaptic targets in the olfactory bulb are lesioned by NMDA and demonstrate loss of P2-expressing OSNs, our reported loss of OSNs is not accompanied by a reduction in epithelium thickness or cellular signs of atrophy. A general increased level of G-protein G_{olf}, indeed, might render the OSNs overactive and disrupt normal activity-dependent mechanisms involved in the formation of a precise olfactory sensory map leading to the formation of heterogeneous glomeruli. In this context, it is interesting to recall that a transgenic line of mice (caG_s^{hi} mice) with excessive cAMP signals also produced glomeruli with heterogeneous populations of axons expressing different ORs (Imai et al., 2006).

In conclusion, we have demonstrated that coding of olfactory information can be modulated through deletion of a major voltage-dependent K channel in the olfactory bulb to alter the peripheral expression of ORs and the refinement of pursuant synaptic connections. Neural maps are derived from chemical guidance cues and electrical activity. In the olfactory system, as demonstrated for other sensory modalities, neural activity plays an important role in fine tuning the transduced external information. Explicitly in the olfactory system, we now know that neural activity in mitral cells or higher central nervous system neurons regulates homogeneous glomerular formation, assists in pruning of extranumerary connections to stabilize the synapse, and controls the abundance of OSNs at the periphery. In future experiments it will be exciting to discover whether mitral cells are providing feedback information to OSNs to either stabilize or destabilize their connections within a glomerulus, perhaps involving "interdependence interaction" or even affecting OSN survival. In sum, once the glomerulus is established, interdependent interaction of similar axons and voltage-dependent activity of postsynaptic projection neurons may act like proofreading mechanisms to maintain the precise connectivity inherent in an olfactory sensory map.

ACKNOWLEDGMENTS

We thank Ms. Kimberly Riddle for imaging assistance through the Florida State University Microscopy Core Facility in the Department of Biological Science and Ms. Danielle Walker and Mr. Robert Daly for their assistance with mouse colony maintenance and genotyping, and for routine technical assistance. We also thank Dr. Peter Mombaerts for his donation of the odorant receptor-tagged mice that were essential to our project. We are grateful for the extremely generous contributions of antisera for our investigation by Drs. Heinz Breer, Richard Axel, and Albert Farbman. We thank Mr. Charles Badland for expert graphic assistance in the preparation of our figures.

LITERATURE CITED

Ardiles Y, de la Puente R., Toledo R, Isgor C, Guthrie K. 2007. Response of olfactory axons to loss of synaptic targets in the adult mouse. Exp Neurol, doi:10.1016/j.expneurol.2007.06.022.

Baker H, Grillo M, Margolis FL. 1989. Biochemical and immunocytochemical characterization of olfactory marker protein in the rodent central nervous system. J Comp Neurol 285:246–261.

Balu R, Larimer P, Strowbridge BW. 2004. Phasic stimuli evoke precisely timed spikes in intermittently discharging mitral cells. J Neurophysiol 92:743–753.

Barnea G, O'Donnell S, Mancia F, Sun X, Nemes A, Mendelsohn M, Axel R. 2004. Odorant receptors on axon termini in the brain. Science 304: 1468.

Belluscio L, Gold GH, Ngai J. 1998. Mice deficient in G(olf) are anosmic. Neuron 20:69–81.

Belluscio L, Lodovichl C, Feinstein P, Mombaerts P, Katz L. 2002. Odorant receptors instruct functional circuitry in the mouse olfactory bulb. Nature 419:296–300.

Biju KC, Walker DM, Fadool DA. 2006. Gene-targeted deletion of Kv1.3 channel alters olfactory receptor gene expression and modifies primary olfactory projections. Chem Senses 31:A135. Abstract.

Bozza T, Feinstein P, Zheng C, Mombaerts P. 2002. Odorant receptor expression defines functional units in the mouse olfactory system. J Neurosci 22:3033–3043.

Brunet LJ, Gold GH, Ngai J. 1996. General anosmia caused by a targeted disruption of the mouse olfactory cyclic nucleotide-gated ion channel. Neuron 17:681–693.

Buiakova OI, Baker H, Scott JW, Farbman A, Kream R, Grillo M, Franzen L, Richman M, Davis LM, Abbondanzo S, Stewart CL, Margolis FL. 1996. Olfactory marker protein (OMP) gene deletion causes altered physiological activity of olfactory sensory neurons. Proc Natl Acad Sci U S A 94:9858–9863.

Bulfone A, Wang F, Hevner R, Anderson S, Cutforth T, Chen S, Meneses J, Pedersen R, Axel R, Rubenstein JLR. 1998. An olfactory sensory map develops in the absence of normal projection neurons or GABAergic interneurons. Neuron 21:1273–1282.

Callahan CA, Thomas JB. 1994. Tau-beta-galactosidase, an axon-targeted fusion protein. Proc Natl Acad Sci U S A 91:5972–5976.

Chehrehasa F, St. John JA, Key B. 2006. Implantation of a scaffold following bulbectomy induces laminar organization of regenerating olfactory axons. Brain Res 1119:58–64.

Colley B, Biju KC, Visegrady A, Campbell S, Fadool DA. 2007. TrkB increases Kv1.3 ion channel half-life and surface expression. Neuroscience 144:531–546.

Cook KK, Fadool DA. 2002. Two adaptor proteins differentially modulate the phosphorylation and biophysics of Kv1.3 ion channel by SRC kinase. J Biol Chem 277:13268–13280.

Cramer KS, Sur M. 1995. Activity-dependent remodeling of connections in the mammalian visual system. Curr Opin Neurobiol 5:106–111.

Dawes CJ. 1984. Biological techniques for transmission and scanning electron microscopy. Burlington, VT: Ladd Research Industries.

Doupnik CA, Davidson N, Lester HA. 1995. The inward rectifier potassium channel family. Curr Opin Neurobiol 5:268–277.

Ebrahimi FA, Chess A. 2000. Olfactory neurons are interdependent in maintaining axonal projections. Curr Biol 10:219–222.

Fadool DA, Tucker K, Phillips JJ, Simmen JA. 2000. Brain insulin receptor causes activity-dependent current suppression in the olfactory bulb through multiple phosphorylation of Kv1.3. J Neurophysiol 83:2332–2348.

Fadool DA, Tucker K, Perkins R, Fasciani G, Thompson RN, Parsons AD, Overton JM, Koni PA, Flavell RA, Kaczmarek LK. 2004. Kv1.3 channel gene-targeted deletion produces "Super-Smeller Mice" with altered glomeruli, interacting scaffolding proteins, and biophysics. Neuron 41: 389–404.

Feinstein P, Mombaerts P. 2004. A contextual model for axonal sorting into glomeruli in the mouse olfactory system. Cell 117:817–831.

Feinstein P, Bozza T, Rodriguez I, Vassalli A, Mombaerts P. 2004. Axon guidance of mouse olfactory sensory neurons by odorant receptors and the B2 adrenergic receptor. Cell 117:833–846.

Fitzsimond RM, Poo MM. 1998. Retrograde signaling in the development and modification of the synapse. Physiol Rev 78:143–170.

Graziadei PP, Levine RR, Graziadei GA. 1978. Regeneration of olfactory axons and synapse formation in the forebrain after bulbectomy in neonatal mice. Proc Nat Acad Sci U S A 75:5230–5234.

Graziadei PP, Levine RR, Monti Graziadei GA. 1979. Plasticity of connections of the olfactory sensory neuron: regeneration into the forebrain following bulbectomy in the neonatal mouse. Neuroscience 4:713–727.

Hahm J, Cramer KS, Sur M. 1999. Pattern formation by retinal afferents in the ferret lateral geniculate nucleus: developmental segregation and the role of N-methyl-D-aspartate receptors. J Comp Neurol 411:327–345.

Hooks BM, Chen C. 2006. Distinct roles for spontaneous and visual activity in remodeling of the retinogeniculate synapse. Neuron 52:281–291.

Imai T, Suzuki M, Sakano H. 2006. Odorant receptor-derived cAMP signals direct axonal targeting. Science 314:657–661.

Ivic L, Pyrski MM, Margolis JW, Richards LJ, Firestein S, Margolis FL. 2000. Adenovirus vector-mediated rescue of the OMP-null phenotype *in vivo*. Nat Neurosci 3:1113–1120.

Jones DT, Reed RR. 1989. G_{olf}: an olfactory neuron specific-G protein involved in odorant signal transduction. Science 244:790–795.

Katz LC, Shatz CJ. 1996. Synaptic activity and the construction of cortical circuits. Science 274:1133–1138.

Keller A, Margolis FL. 1975. Immunological studies of the rat olfactory marker protein. J Neurochem 24:1101–1106.

Kerr MA, Belluscio L. 2006. Olfactory experience accelerates glomerular refinement in the mammalian olfactory bulb. Nat Neurosci 9:484–486.

Koni PA, Khanna R, Chang MC, Tang MD, Kaczmarek LK, Schlichter LC, Flavella RA. 2003. Compensatory anion currents in Kv1.3 channel-deficient thymocytes. J Biol Chem 278:39443–39451.

Kues WA, Wunder F. 1992. Heterogeneous expression patterns of mammalian potassium channel genes in developing and adult rat brain. Eur J Neurosci 4:1296–1308.

Lattemann M, Zierau A, Schulte C, Seidl S, Kuhlmann B, Hummel T. 2007. Semaphorin-1a controls receptor neuron-specific axonal convergence in the primary olfactory center of *Drosophila*. Neuron 53:169–184.

LeVay S, Wiesel TN, Hubel DH. 1980. The development of ocular dominance columns in normal and visually deprived monkeys. J Comp Neurol 191:1–51.

Lin DM, Wang F, Lowe G, Gold GH, Axel R, Ngai J, Brunet L. 2000. Formation of precise connections in the olfactory bulb occurs in the absence of odorant-evoked neuronal activity. Neuron 26:69–80.

Lin W, Arellano J, Slotnick B, Restrepo D. 2006. Odors detected by mice deficient in cyclic nucleotide-gated channel subunit A2 stimulate the main olfactory system. J Neurosci 24:3703–3710.

Lin W, Margolskee R, Donnert G, Hell SW, Restrepo D. 2007. Olfactory neurons expressing transient receptor potential channel M5 (TRPM5) are involved in sensing semiochemicals. Proc Natl Acad Sci U S A 104:2471–2476.

Long JE, Garel S, Depew MJ, Tobet S, Rubenstein JLR. 2003. DLX5 regulates development of peripheral and central components of the olfactory system. J Neurosci 23:568–578.

López-Mascaraque L, García C, Blanchart A, De Carlos JA. 2005. Olfactory epithelium influences the orientation of mitral cell dendrites during development. Dev Dynamics 232:325–335.

Mania-Farnell B, Farbman AI. 1990. Immunohistochemical localization of guanine nucleotide-binding proteins in rat olfactory epithelium during development. Brain Res Dev Brain Res 51:103–112.

Marks DR, Fadool DA. 2007. Post-synaptic density (PSD-95) perturbs insulin-induced Kv1.3 channel modulation via a clustering mechanism involving the SH_3 domain. J Neurochem 103:1068–1627.

Menco BP, Tekula FD, Farbman AI, Danho W. 1994. Developmental expression of G-proteins and adenylyl cyclase in peripheral olfactory systems. Light microscopic and freeze-substitution electron microscopic immunocytochemistry. J Neurocytol 23:708–727.

Mombaerts P. 1996. Targeting olfaction. Curr Opin Neurobiol 6:481–486.

Mombaerts P. 2006. Axonal wiring in the mouse olfactory system. Annu Rev Cell Dev Biol 22:713–737.

Mombaerts P, Wang F, Dulac C, Chao SK, Nemes A, Mendelsohn M, Edmondson J, Axel R. 1996. Visualizing an olfactory sensory map. Cell 87:675–686.

Mori K, Nagao H, Yoshihara Y. 1999. The olfactory bulb: coding and processing of odor molecule information. Science 286:711–715.

Mountford PS, Smith AG. 1995. Internal ribosome entry sites and dicistronic RNAs in mammalian transgenesis. Trends Genet 11:179–184.

Nakatani H, Serizawa S, Nakajima M, Imai T, Sakano H. 2003. Developmental elimination of ectopic projection sites for the transgenic OR gene that has lost zone specificity in the olfactory epithelium. Eur J Neurosci 18:2425–2432.

Ressler KJ, Sullivan SL, Buck L. 1993. A zonal organization of odorant receptor gene expression in the olfactory epithelium. Cell 73:597–609.

Royal SJ, Key B. 1999. Development of P2 olfactory glomeruli in P2-internal ribosome entry site-tau-LacZ transgenic mice. J Neurosci 19: 9856–9864.

Sammeta N, Yu T, Bose SC, McClintock TS. 2007. Mouse olfactory sensory neurons express 10,000 genes. J Comp Neurol 502: 1138–1156.

St. John JA, Key B. 2005. Olfactory marker protein modulates primary olfactory axon overshooting in the olfactory bulb. J Comp Neurol 488: 61–69.

St. John JA, Clarris HJ, Key B. 2002. Multiple axon guidance cues establish the olfactory topographic map: how do these cues interact? Int J Dev Biol 46:639–647.

St. John JA, Clarris HJ, McKeown S, Royal S, Key B. 2003. Sorting and convergence of primary olfactory axons are independent of the olfactory bulb. J Comp Neurol 464:131–140.

Storan MJ, Key B. 2004. Target tissue influences the peripheral trajectory of mouse primary sensory olfactory axons. J Neurobiol 61:175–188.

Strotmann J, Conzelmann S, Beck A, Feinstein P, Breer H, Mombaerts P. 2000. Local permutations in the glomerular array of the mouse olfactory bulb. J Neurosci 20:6927–6938.

Strotmann J, Levai O, Fleischer J, Schwarzenbacher K, Breer H. 2004. Olfactory receptor proteins in axonal processes of chemosensory neurons. J Neurosci 24:7754–7761.

Sweeney LB, Couto A, Chou Y-H, Berdnik D, Dickson BJ, Luo L, Komiyama T. 2007. Temporal target restriction of olfactory receptor neurons by semaphorin-1a/plexinA-mediated axon-axon interactions. Neuron 53:185–200.

Szabò I, Adams C, Gulbins E. 2004. Ion channels and membrane rafts in apoptosis. Pflugers Arch 448:304–312.

Treloar HB, Tomasleqicz H, Magnuson T, and Key B. 1997. The central pathway of primary olfactory axons is abnormal in mice lacking the N-CAM-180 isoform. J Neurosci 32:643–658.

Tsuboi A, Yoshihara S-I, Yamazaki N, Kasai H, Asai-Tsuboi H, Komatsu M, Serizawa S, Ishii T, Matsuda Y, Nagawa F, Sakano H. 1999. Olfactory neurons expressing closely linked and homologous odorant receptor genes tend to project their axons to neighboring glomeruli on the olfactory bulb. J Neurosci 19:8409–8418.

Tucker K, Fadool DA. 2002. Neurotrophin modulation of voltage-gated potassium channels in rat through TrkB receptors is time and sensory experience dependent. J Physiol 542:413–429.

Tucker K, Overton JM, Fadool DA. 2007. Kv1.3 gene-targeted deletion reduces fat deposition and total body weight in melanocortin 4 receptor (MC4R)-null mice; a model of hypothalamic-driven late-onset obesity. Appetite 49(1):336. Abstract.

Vassar R, Ngai J, Axel R. 1993. Spatial segregation of odorant receptor expression in the mammalian olfactory epithelium. Cell 74:309–318.

Walters E, Grillo M, Oestreicher AB, Margolis FL. 1996. LacZ and OMP are co-expressed during ontogeny and regeneration in olfactory receptor neurons of OMP promoter-lacZ transgenic mice. Int J Dev Neurosci 14:813–822.

Wang F, Nernes A, Mendelsohn M, Axel R. 1998. Odorant receptors govern the formation of a precise topographic map. Cell 93:47–60.

Xu J, Koni PA, Wang P, Li G, Kaczmarek LK, Wu Y, Li Y, Flavell RA, Desir GV. 2003. The voltage-gated potassium channel Kv1.3 regulates energy homeostasis and body weight. Hum Mol Genet 12:551–559.

Youngentob SL, Margolis FL. 1999. OMP gene deletion causes an elevation in behavioral threshold sensitivity. Neuroreport 10:15–19.

Youngentob SL, Margolis FL, Youngentob LM. 2001. OMP gene deletion results in an alteration in odorant quality perception. Behav Neurosci 115:626–631.

Yu CR, Power J, Barnea G, O'Donnell S, Brown HEV, Osborne J, Axel R, Gogos JA. 2004. Spontaneous neural activity is required for the establishment and maintenance of the olfactory sensory map. Neuron 42: 553–566.

Zheng C, Feinstein P, Bozza T, Rodriguez I, Mombaerts P. 2000. Peripheral olfactory projections are differentially affected by mice deficient in a cyclic nucleotide-gated channel subunit. Neuron 26:81–91.

Zou D-J, Feinstein P, Rivers AL, Mathews GA, Kim A, Greer CA, Mombaerts P, Firestein S. 2004. Postnatal refinement of peripheral olfactory projections. Science 304:1976–1979.